Biovigilance Toolbox for Nationwide Biosurveillance of Air-borne Plant Pathobiome: Environmental and Landscape Drivers of Airborne Cereal Pathogens

By Morgan Bakelmun

Thesis submitted to the University of Ottawa

in partial Fulfillment of the requirements for the Master's degree in Biology Specialization in Bioinformatics

Department of Biology

Faculty of Science

University of Ottawa

Abstract

Fungal pathogens pose a constant threat to Canadian cereal production by reducing yield and grain quality. Many of these pathogens disperse via air currents, enabling rapid, long-distance spread. Moving beyond reactive disease management, this study employs a biovigilance framework to characterize and predict pathogen dynamics. We tested three primary hypotheses: that airborne pathogen distribution is driven by host-crop availability (spatial hypothesis), regulated by specific meteorological conditions (temporal hypothesis), and that species-level resolution reveals ecological patterns obscured at the genus level (taxonomic resolution hypothesis). Seven air samplers were deployed across seven provinces from 2020 to 2023, collecting 437 samples. Using ITS2 metabarcoding and the AODP bioinformatic pipeline, we generated 14.4 million high-quality reads. We identified 43 ASVs representing 15 species of cereal-associated pathogens. Supporting the spatial hypothesis, the wheat specialist *Parastagonospora nodorum* and various *Ustilago* species exhibited distributions strictly coupled with the prevalence of their respective host crops. In support of the temporal hypothesis, *Fusarium*, *Blumeria graminis*, and *Puccinia* species displayed climate-responsive dynamics, with abundance modulated by humidity and wind speed. Furthermore, consistent with our taxonomic resolution hypothesis, resolving pathogens to the species level allowed us to distinguish host-specific dispersal patterns within complex genera like *Ustilago*. This study demonstrates that integrating high-resolution airborne metabarcoding with landscape and climatic data provides a scalable framework for predictive disease surveillance and targeted intervention in complex agroecosystems. The pronounced seasonal peaks of *Blumeria graminis* associated with relative humidity and host presence within a 5 km radius further validate the temporal hypothesis, linking environmental suitability with host availability. This study

demonstrates that integrating high-resolution airborne metabarcoding with landscape and climatic data can pinpoint high-risk periods and locations, offering a scalable framework for predictive disease surveillance and targeted intervention in complex agroecosystems.

Keywords: Plant pathogens; DNA metabarcoding; cereal crops; biovigilance; host preference; climatic drivers

Résumé

Les champignons pathogènes constituent une menace constante pour les cultures canadiennes, car ils réduisent les rendements et la qualité des récoltes et mettent en danger la santé des consommateurs. Plusieurs d'entre eux sont disséminés par les courants d'air, ce qui leur permet d'infecter de vastes zones et de se propager rapidement sur de longues distances. Plutôt de faire contre ces ravageurs quand une épidémie se déclare, la biovigilance vise à prévoir et à prévenir la propagation de ces agents pathogènes. Sept échantillonneurs d'air ont été déployés dans sept provinces durant la saison de croissance 2020-2023, permettant le prélèvement de 437 échantillons. Grâce au métabarcoding de la région ITS2, plus de 14,4 millions de séquences de haute qualité ont été obtenues, couvrant 4 650 ASV et 976 genres. Dix genres pathogènes d'intérêt ont été sélectionnés, 43 ASV ont été identifiés comme pathogènes associés aux céréales, appartenant à 7 genres et 15 espèces. *Parastagonospora nodorum*, un spécialiste du blé, a présenté des pics marqués au début de l'été dans les régions de prairies, au moment de la floraison du blé. En revanche, chaque espèce d'*Ustilago* a affiché des schémas spatiaux spécifiques à l'espèce, correspondant à sa céréale hôte respective. Le *Fusarium* a présenté une grosse distribution (sensible aux variations climatiques), sur différents sites et au fil des ans, reflétant de sa polyvalence écologique. Les facteurs atmosphériques, notamment l'humidité et le vent, ont modulé la dynamique de dispersion, contribuant aux pics de fin de saison des espèces de *Blumeria graminis* et de *Puccinia*, selon le site et l'année. Cette étude démontre que l'intégration du métabarcoding à haute résolution avec des données paysagères et climatiques permet de repérer les périodes et les lieux à haut risque, offrant ainsi un cadre évolutif pour la surveillance prédictive des maladies et l'intervention ciblée dans les agroécosystèmes complexes.

Mots-clés: Pathogènes végétaux ; métabarcoding d'ADN ; cultures céréalières ; biovigilance ; préférence d'hôte ; facteurs climatiques

Acknowledgements

I would first like to thank my supervisor Dr. Wen Chen for giving me this opportunity in the first place. I also wish to thank my Thesis Advisory Committee members and examiners; Dr. Stéphane Aris-Brosou, Dr. Guillame Bilodeau, Dr. Kelly Burkett, and Dr. Leonardo Galindo Gonzalez. I have been very grateful for your help both on this project and for developing my career.

I want to thank the research teams of Dr. Rishi Burlakoti, Dr. Odile Carisse, Dr. Syama Chatterton, Dr. Yong Min Kim, Dr. Kui Liu, Dr. Ali Shawkat for performing the data collection at each of the different sites. I also want to thank Philip Pham for collecting the data at the Ontario sites before I joined the project.

I must also acknowledge Agriculture and Agrifoods Canada for the funding of this project, for while my time is free food is not.

And finally, I must thank my fellow researchers in the Chen Lab; Ishraq Akbar, Cecily Costain, and Cecilio Valadez-Cano. A very special thanks to Yichao Shi, whose tireless reviews of my work kept me on track to complete this thesis. I do not think I could have completed this without your oversight, so thank you very much for all you have done.

Table of Contents

Table of Figures and Tables

Author Contributions

A manuscript based on this project was prepared by Bakelmun M., Shi Y., Pham P., Van Der Heyden H., Bilodeau G., Chatterton S., Burlakoti R., Shawkat A., Kim Y.M., Liu K., Lapen D.R., Sunohara M., Craiovan E., and Chen W. (2026) titled “Host availability and environmental conditions jointly structure airborne cereal pathogen communities across Canadian agroecosystems”. Contributions are as follows.

Conceptualization: W.C.

Methodology: W.C., P.P., M.B.

Data Collection: P.P., S.C., R.B., A.S, Y.M.K., K.L., D.R.L., M.S, E.C.

Software: M.B., W.C.

Data processing: M.B.

Data analysis: M.B., Y. S.

Writing: M.B.

Editing and review: Y.S., W.C.

Supervision: W.C., Y.S.

Funding acquisition: W.C.

1. Introduction

1.1 Cereal Crops

Cereal crops are an important part of the global food supply, serving as a major source of carbohydrates, fibers, and proteins for both humans and livestock. In Canada, wheat (*Triticum aestivum* L., T. durum L.), barley (*Hordeum vulgare* L.), oat (*Avena sativa* L.), and corn (*Zea mays* L.) occupy over 40% of all arable cultivated land and produce more than 47 million tons of feed annually (Stat Canada, 2024). The Prairie provinces, Ontario, and Quebec are the primary regions for producing these cereals, benefiting from their fertile soils and cool growing seasons. Despite continuous improvements in pest-resistant crop strains and agronomic practices, fungal diseases continue to cause damages to cereal crop yield, grain quality, and long-term sustainability. Since the turn of the century, fungal pathogens have emerged as the primary microbial threat to agriculture, driving an estimated 11.2% to 12.8% baseline reduction in annual cereal yields, and can escalate up to 50% during severe epidemics (Moore, 2020; Różewicz et al., 2021; Savary et al., 2017).

Agricultural systems face increasing challenges to effective crop protection. Climate change is reducing host crop fitness and altering pest dynamics, dispersal patterns, and interactions with natural enemies through shifts in temperature, moisture, and extreme weather events (Elad & Pertot, 2014; Gautam et al., 2013; Loo, 2009). Global movement of plant materials continues to introduce novel and invasive pests, while certain conventional practices, such as intensive fertilizer use, soil degradation, and repeated pesticide applications, create favourable environments for pathogen proliferation and accelerate the evolution of pesticide-resistant strains. At the same time, consumer demand for reduced-pesticide or

pesticide-free food products is rising (Sawyer et al., 2008). Even with large-scale production systems, resistant cultivars, and moderate chemical inputs, fungal pathogens continue to pose significant threats to the productivity and resilience of Canadian field crops. Recent reviews of Prairie phytopathogens highlight the persistent and emerging challenges affecting cereals, oilseeds, and pulse crops across the region (McCallum et al., 2021). As a major exporter of agricultural commodities, Canada requires robust pathogen surveillance systems capable of assessing pest biology, distribution, economic impact, and mitigation options.

1.2. Cereal Pathogens & Dispersal

Cereal fungal diseases in Canada can be broadly classified into three groups: necrotrophic, biotrophic, and inflorescence-infecting groups (Moore et al. 2020). Each has different strategies for infection and host interaction. Necrotrophic fungi, such as *Zymoseptoria tritici*, *Parastagonospora nodorum*, *Pyrenophora tritici repentis*, *Rhynchosporium commune*, and *Bipolaris sorokiniana*, cause foliar and basal diseases such as *Septoria tritici* blotch, *Septoria nodorum* blotch, tan spot, net blotch, barley leaf scald, and common root rot (Zhan et al. 2014; Fernandez et al. 2016; Kutcher et al. 2018; Elmhirst 2023). These pathogens actively attack living cells, particularly senescing tissues and promote host cell death, with disease severity strongly influenced by moisture, temperature, and residue management, particularly under conservation tillage and continuous cereal rotations (Fernandez et al. 2016; Kutcher et al. 2018; Elmhirst 2023). Biotrophic pathogens, such as by *Blumeria graminis* (powdery mildew) and several *Puccinia* species, including P. *graminis* (stem rust), P. *triticina* (leaf rust), P. *striiformis* (stripe rust), and P. *coronata* (crown rust) are parasitic and depend on living host tissue, causing some of the most damaging foliar diseases of cereals (Lorrain et al. 2019; Mapuranga et al. 2022). Their airborne urediniospores enable rapid spread under moderate temperatures and

prolonged leaf wetness (Chen et al. 2014; Cowger et al. 2016; Chen et al. 2022). Inflorescence infecting fungi include *Fusarium graminearum*, F. *culmorum*, and F. *avenaceum* (Fusarium head blight); *Claviceps purpurea* (ergot); *Tilletia caries*, T. *foetida*, and T. *controversa* (common and dwarf bunt); and *Ustilago tritici*, U. *nuda*, and U. *hordei* (loose and covered smuts). These pathogens infect flowering and fruiting bodies, disrupting grain formation and reducing kernel quality (Carris et al. 2006; Miedaner and Geiger 2015; Ferrigo et al. 2016; Mohite et al. 2025). Additionally, several species (particularly *Fusarium* and *Claviceps*) also pose significant food and feed safety risks due to the accumulation of trichothecenes, zearalenone, and ergot alkaloids (Miedaner and Geiger 2015; Ferrigo et al. 2016). Collectively, these fungal taxa represent the principal agents of disease in Canadian cereal systems and are closely tied to both local agronomic practices and larger climatic drivers (Fernandez et al. 2016; Elmhirst 2023).

Airborne dispersal is therefore one of the most important dissemination pathways of most cereal fungal pathogens. The atmosphere serves as a major conduit for fungal dispersal, enabling spores ranging from 0.1–100 μm to travel long distances and initiate outbreaks far from their source (Stakman & Christensen, 1946). Spores of *Puccinia*, *Fusarium*, *Zymoseptoria*, and *Pyrenophora* are capable of translocation via prevailing winds. This allows for long distance pathogen migration between fields and even across continents (Golan and Pringle 2017; Chen et al. 2022).

1.3. Biovigilance

These pressures have driven the development of biovigilance-based approaches to crop disease management (Magarey et al., 2009). Biovigilance in plant pathology, as coined by Carisse et al. (2017), provides a proactive framework for detecting, assessing and managing plant health threats before they become epidemics. The framework consists of six interconnected

steps: awareness, detection, assessment, understanding, mitigation, and appropriateness. Awareness involves anticipating potential risks based on existing knowledge; detection refers to identifying the presence of a threat in the environment; assessment focuses on monitoring the threat and determining its significance; understanding requires in-depth study of the organism's biology, dispersal, and vulnerabilities; mitigation involves developing and implementing strategies to reduce risk; and appropriateness ensures that the chosen interventions are effective and do not introduce unintended consequences. Collectively, these steps shift plant disease management from reactive responses during outbreaks toward preventative, evidence-based strategies that reduce the likelihood of epidemic development.

A central component of biovigilance is the surveillance of airborne plant pathogens, which are transported passively or actively through the atmosphere The atmosphere serves as a major conduit for fungal dispersal, Fungal species rely on both passive mechanisms, such as wind, rain splash, and turbulent mixing, and active spore ejection to reach new hosts or infection sites (Van Der Heyden et al., 2021). The atmosphere is therefore both a supply and an early indicator of pathogen presence. Continuous monitoring of airborne spores provides critical forecasts into disease epidemiology and supports the early warning systems central to biovigilance frameworks (Carisse et al. 2017).

1.4. Implementation in the Field (Air Sampling Networks)

Large-scale spore-sampling networks have proven effective for tracking pathogen movement. For example, coordinated monitoring of *Puccinia striiformis* (stripe rust) across the Pacific Northwest and Canadian Prairies has demonstrated how airborne urediniospores can move long distances and initiate early-season epidemics, with spore counts and meteorological data improving regional disease forecasts (Chen et al., 2022; Chen et al., 2014).

Effective surveillance requires appropriate air sampling, such as impaction, cyclone, electrostatic, and virtual impaction systems, to accurately capture and categorize airborne fungal communities (Van Der Heyden et al., 2021). From this aspect, constructing an effective biovigilance platform needs to select appropriate spore-trapping samplers, which ensures accurate representation of the aeromycobiota (Van Der Heyden et al., 2021). Chen et al. (2018) evaluated the effectiveness of three samplers, including active rain, passive rain, and active volumetric air samplers, and provided specific recommendations for their use in detecting and recovering phytopathogens. Key factors such as the sampling period and height significantly influence the detection of airborne spores (Van Der Heyden et al., 2021). Research has shown that spore counts tend to decrease as the sampling height increases (Aylor, 1983; Aylor et al., 2001). To achieve continuous monitoring, some studies employ 7-day samplers, which provide hourly or daily spore counts (Hellin et al., 2018; Reich et al., 2017; Rogers et al., 2009).

1.5. Molecular Detection & Bioinformatics

Advancements in high-throughput sequencing (HTS) have significantly transformed the detection and tracking of plant pathogen dispersal. HTS-based metagenomic approaches—including DNA metabarcoding, shotgun metagenomics, and metatranscriptomics—enable sensitive, multi-taxon characterization of environmental samples. Among these, DNA metabarcoding is the most widely applied for aerobiological surveillance. At a large-scale, cost effectiveness is a factor to consider. For this reason, short-read metabarcoding is preferable. It involves extracting DNA from environmental substrates such as air, soil, or water, amplifying a target barcode region using PCR, and sequencing the resulting amplicons on short- or long-read platforms such as Illumina or Nanopore (Bentley et al., 2008; MacKenzie & Argyropoulos, 2023). Taxonomic composition is then inferred by comparing sequences to reference databases.

Metabarcoding is cost-effective and supports broad recovery of microbial taxa from diverse environmental samples (Chen et al., 2018; Dietzel et al., 2019; Ferguson et al., 2019; E. Karlsson et al., 2020; I. Karlsson et al., 2016). However, short-read metabarcoding often lacks the resolution needed to accurately identify species or sub-species, limiting its effectiveness in detecting phytopathogens, which are typically defined at these levels (Chen et al., 2022).

Internal Transcribes Spacer 2 (ITS2) metabarcoding has improved airborne fungal pathogen surveillance by enabling sensitive, multi-taxon detection from air samples (Banchi et al. 2018; Chen et al. 2022; Chen et al. 2024). Despite its broad fungal coverage, ITS2 alone frequently lacks the resolution needed to distinguish closely related species (Schoch et al. 2012; Chen et al. 2022). Species-level identification is critical because pathogenicity, host specificity, and mycotoxin production often vary among species and even among strains. For example, only certain *Fusarium graminearum* strains produce deoxynivalenol, and subspecies of *Puccinia striiformis* differ in host range and fungicide sensitivity (Fernandez et al. 2016; Chen et al. 2022). The success of short-read metabarcoding depends heavily on the selection of appropriate barcode regions and primers (Chen et al., 2022; Reich et al., 2023). Although the internal transcribed spacer (ITS) region is the most widely used fungal barcode due to its utility in phylogenetic studies, it has well-recognized limitations in resolving closely related species (Banchi et al., 2018; Schoch et al., 2012). Secondary markers such as BT and TEF1-α therefore play an important role in improving taxonomic resolution, particularly when supported by curated reference datasets (Chen et al., 2022). However, the trade-off of it having a wide coverage, high amplification success rates, and its comprehensiveness in bioinformatics tools makes ITS2 more favourable than other markers for short-read metabarcoding (Nilsson et al., 2019; Schoch et al., 2012).

Accurate sequence classification also depends heavily on the availability of high-quality reference databases and robust bioinformatics tools. Taxonomic gaps and inconsistencies in public repositories such as GenBank can hinder identification, especially for groups like rust fungi and oomycetes that are under-represented in existing databases (Hibbett et al., 2016). To address these limitations, curated resources such as the CR-ITS2-refDB for cereal rust fungi (Chen et al., 2022) and the oomycetes-ITS1-refDB (Gahagan et al., 2023) have been developed to improve classification accuracy. Traditional classifiers, such as BLAST, RDP, and q2-feature-classifier, often show limited species-level accuracy for short ITS sequences (<35%) due to high sequence similarity among closely related taxa (Altschul et al., 1990; Eddy, 1995; Edgar, 2010; Wang et al., 2007). The Automated Oligonucleotide Design Pipeline (AODP) (Zahariev et al., 2018) addresses these challenges by extracting signature oligonucleotides unique to target taxa and applying a modified global alignment algorithm, outperforming other classifiers in both precision and recall. Integrating AODP into metabarcoding pipelines enhances species-level identification and strengthens the reliability of airborne pathogen surveillance (Chen et al., 2022; Chen et al. 2024).

An effective biovigilance toolbox also requires identifying the environmental drivers that shape fungal spore dissemination dynamics. Statistical and machine-learning approaches provide powerful tools for disentangling the complex interactions among weather, land use, and spore abundance. Rust fungi, for example, disperse rapidly via airborne urediniospores and are expected to benefit from climate-driven shifts in temperature, humidity, and atmospheric pressure across Canada (Lyon & Broders, 2017). Chen et al. (2024) used Random Forest modelling to show that air temperature and humidity are key predictors of leaf rust spore abundance. Such modelling approaches can reveal hidden patterns in large datasets, improve

predictive accuracy, and adapt as new data become available, thereby enhancing early-warning capabilities.

In conclusion, integrating spore-sampling networks, metabarcoding, and dense ancillary metadata (e.g., weather, land use, crop distribution, and agricultural practices) with statistical and machine-learning models provides a robust foundation for modern plant pathogen monitoring. These interdisciplinary approaches are driving the development of advanced biovigilance platforms that are essential for managing plant diseases and mitigating the impacts of climate change and land-use change on agriculture. As reference databases and bioinformatic tools continue to improve, these innovations will support increasingly precise pathogen detection and more effective disease management strategies.

1.6 Objectives and Hypotheses

The overarching goal of this study is to characterize the temporal and spatial dynamics of the airborne phytopathobiome across Canada's major agricultural landscapes. By integrating nationwide aerobiological monitoring with ITS2 metabarcoding and dense ancillary metadata, this research aims to identify the environmental and landscape drivers of airborne crop pathogens to support a proactive biovigilance framework. Based on the ecological principles of pathogen dispersal and host specificity, this study tests the following hypotheses:

1. **Spatial Hypothesis:** The spatial distribution and relative abundance of airborne cereal-associated pathogens are primarily driven by the local landscape composition and the prevalence of their specific host crops.
2. **Temporal Hypothesis:** The seasonal dispersal dynamics of airborne pathogens are regulated by specific meteorological conditions (such as humidity, temperature, and

wind) and will align temporally with the phenological development stages of their host crops.

3. **Taxonomic Resolution Hypothesis:** Resolving pathogen taxa to the species level will reveal distinct spatial and temporal ecological patterns that are otherwise obscured when analyzed at the broader genus level.

To test these hypotheses, the specific objectives of this study are to:

(i) Characterize the spatial and temporal dynamics of ten major cereal-associated fungal pathogen genera across multiple sentinel sites in Canada's major cereal-producing regions.

(ii) Identify and quantify the specific environmental factors—encompassing both weather patterns and land use/crop distribution—that influence their airborne dispersal and seasonal abundance.

(iii) Resolve targeted pathogens to the species level using advanced bioinformatic pipelines to improve the accuracy of species-specific disease risk assessments and spatial-temporal tracking.

2. Materials & Methods

2.1 Experimental design, sampling sites, and metadata collection

In this study, air samples were collected by scientists from Agriculture and Agri-Food Canada (AAFC)'s several Research Centres across Canada. A total of 7 air samplers were deployed in seven provinces (Figure 1). Air sampling was carried out during the growing seasons of 2020-2023 at the BC site, 2021-2023 at AB, ON, QC and NS sites, 2022-2023 at the MB and SK sites.

Air samples were collected using cyclone samplers (Burkard Manufacturing Co. Ltd., Richmansworth, England), which is a non-filter-based system designed for collecting air-dispersed particulate matter directly into a sterile 1.5-ml microcentrifuge tube in the field. The cyclone samplers are typically used for collecting airborne dry particles but can also capture water samples during rainy weeks. The samplers were deployed to the field according to the duration of growing seasons of local crops, usually from the spring (April or May) to the harvest in the fall (September, October or November). Samples were collected weekly after 7 days of field exposure. On each sampling day, the microcentrifuge tubes containing the samples were brought to the laboratory, and new tubes were installed in the samplers. A total of 437 air samples were collected from all sites between 2020 and 2023.

For all sites, climatological data was obtained from Environment and Climate Change Canada's meteorological service (http://climate.weather.gc.ca/). This included temperature-related variables such as average temperature, minimum temperature, maximum temperature, wind direction (in 10s of degrees from north), maximum wind speed (in kilometers per hour), and precipitation (in millimeters). For each site, the closest weather station with hourly data was

selected. The closest weather station to a sampling site was 0.01 kilometers away (at ON1) while the furthest was 7.57 kilometers away (QC07), with a mean distance of 2.22 kilometers. Crop cover information within 1 km, 2 km, 5 km, and 20 km radii around each sampling site was extracted from the annual crop inventory compiled by Agriculture and Agri-Food Canada (https://agriculture.canada.ca/atlas/data_donnees/annualCropInventory/) using QGIS (version 3.42.1) (Dawson et al., 2026).

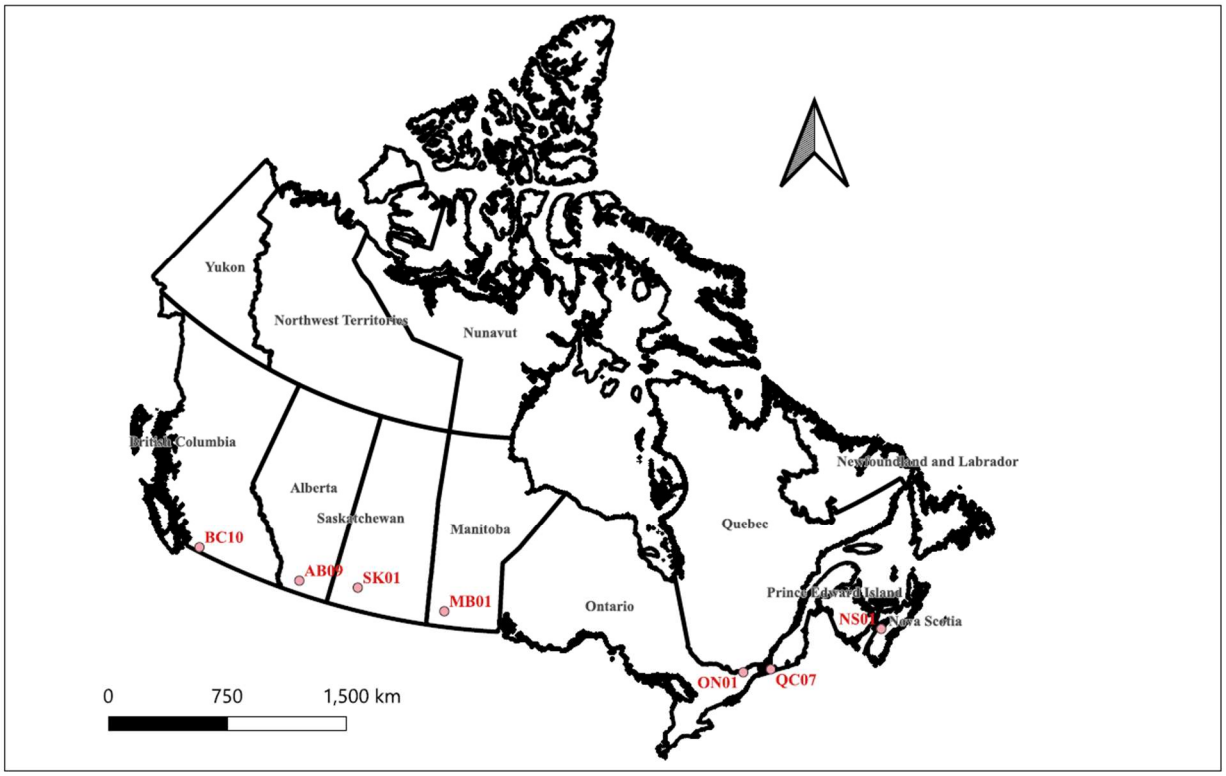

Figure 1. Locations of the sampling sites across Canada. Provincial and territorial boundaries were obtained from Statistics Canada (2021) at https://www12.statcan.gc.ca/census-recensement/2021/geo/sip-pis/boundary-limites/index2021-eng.cfm?year=21.

2.2 DNA extraction

Air samples were collected by collaborators at each location and stored at -80 ℃. At the end of each sampling season, the samples were shipped on dry ice via overnight courier to the Chen lab

at AAFC Ottawa and stored at -80 ℃ until further processing. Genomic DNA was extracted using the DNeasy PowerSoil Pro DNA extraction kit (Qiagen, Hilden, Germany), with modifications. For samples containing rainwater, 10 mM Tris buffer (pH 7.0 to 8.0) was first added to a final volume of 1 ml, and the samples were dried in a Savant DNA 120 SpeedVac concentrator (Thermo Fisher Scientific, Waltham, MA, USA). All the samples were then processed using the same protocol. PowerBead and CD1 solution were added to the sample tubes. The samples were incubated at 65 °C for 5 minutes then sonicated for 1 minute, and this process was repeated twice. After a brief spin in a microcentrifuge, two layers of parafilm were applied to both the inside and outside of the tube lids to prevent spillage during homogenization. The samples were then homogenized in the Precellys ® 24 instrument at 4000 rpm for 20 seconds, repeated twice. The subsequent steps followed the manufacturer's protocol. DNA concentration was measured using a Qubit 3.0 or Qubit Flex fluorometer, and DNA quality was assessed by electrophoresis on a 1% agarose gel. DNA samples were stored at -80 °C for further analysis.

2.3 Library preparation and Illumina Sequencing

Library preparation and DNA sequencing were performed in different batches at three sequencing facilities: Génome Québec Innovation Centre (2021 samples), IMR at Dalhousie University (2020 and 2022 samples), and National Research Council of Canada (2023 samples). Forward primer was ITS3_KYO1 (5'-AHCGATGAAGAACRYAG-3') and the reverse was ITS4rust (5'-CTTATTGATATGCTTAAGTTCAG-3') as this primer pair was shown to have good coverage in the past (Chen et al., 2022). The protocols were similar for each sequencing organization, but slight differences are noted where relevant.

At Genome Quebec Innovation Centre, PCR was performed using the Hot Start High-Fidelity DNA Polymerase and buffer on a BioRad T1 Cycler and included a negative control to detect potential contamination or unintended amplification. This protocol was the same for all primer pairs. The DNA template was diluted to 20 to 50 ng/μL. The initial PCR amplification was carried out in a 24-μL reaction volume comprising 1× PCR buffer with 15 mM MgCl2 (Qiagen, Germantown, MD), 5% DMSO (Roche, Mississauga, ON, Canada), 0.2 mM dNTP mix (FroggaBio, Wheatfield, NY), 0.02 U/μL HotStarTaq DNA polymerase (Qiagen), 0.6 μM of each forward (tagged with D01) and reverse (tagged with D02) primers, 1 μL of DNA template, and 5.51 μL of H2O. The following program was used for amplification: 96°C for 15 min for initial melting; 33 cycles of 96°C for 30 seconds, 52°C for 30 seconds, and 72°C for 60 seconds; and 72°C for 10 minutes. The amplicons were verified on a 2% agarose gel and were purified with sparQ PurMag Beads (Quantabio, Beverly, MA). A secondary PCR was then carried out to add dual indexed barcoded adapters with primers targeting D01 and D02 of the initial PCR products. The PCR was carried out in a 17-μL reaction volume containing 1x PCR 10x buffer without MgCl2 (Roche), 1.8 mM MgCl2, 5% DMSO, 0.2 mM dNTP mix (FroggaBio), 0.025 U/μL FastStart Taq DNA Polymerase (Roche), 12.06 μL of H2O, 2 mM of dual-indexed barcoded adapters, and 1 μL of template. The PCR cycling parameters were 95°C for 10 minutes for initial melting; 15 cycles of 95°C for 15 seconds, 60°C for 30 seconds, and 72°C for 60 seconds; and 72°C for 3 minutes. The secondary PCR products were quantified with a Quant-iT PicoGreen dsDNA Assay Kit (Life Technologies, Carlsbad, CA), pooled with the same quantity from each sample, and then purified with sparQ PureMag Beads (Quantabio). The sequencing libraries were then quantified with Kapa Illumina GA with Revised Primers-SYBR Fast Universal kit (Kapa Biosystems, Woburn, MA). The average fragment size was determined with a LabChip

GX (PerkinElmer, Waltham, MA) instrument. The Phix control library was added to the amplicon pool at a final concentration of 8 pM. The sequencing was performed on an Illumina MiSeq platform in a 2 x 300-bp paired-end format with a v3 600-cycle MiSeq Reagent Kit.

At the Integrated Microbiome Resources Centre, Dalhousie University, the library preparation protocol was originally described by Comeau et al. (2017) and updated by Comeau and Kwawukume (2022). A dual-indexing, one-step PCR was performed using complete "fusion primers", which incorporate Illumina Nextera adaptors, indices, and region-specific primers. A 20-µL reaction was carried out, comprising 4 µL 5× Phusion Plus buffer, 0.4 µL of 40 mM dNTP, 0.4 µL of 1 µM each forward and reverse primers, 0.2 µL of Phusion Plus (2 U/µL), 2 µL of DNA template, and 5.4 µL of H2O. The following thermal cycling conditions were used for amplification: 98°C at 30 seconds for initial denaturation; 25 cycles of 98°C for 10 seconds, 55°C for 30 seconds, and 72°C for 30 seconds; followed by a final extension at 72°C for 4.5 minutes. The resulting PCR products were verified by electrophoresis using an E-Gel 96 (Invitrogen) in a Mother E-Base (Thermo Fisher Scientific) for 12 minutes. Amplicons were subsequently purified and normalized in a single step using the high-throughput Invitrogen SequalPrep 96-well plate kit (Charm Biotech). Purified PCR products were pooled to create a single library, which was quantified using the Invitrogen Qubit dsDNA HS Assay (Thermo Fisher Scientific) prior to sequencing. A PhiX control library was spiked into the amplicon pool at a final concentration of 14 pM. Sequencing was performed on the Illumina MiSeq platform using the v3 600-cycle kit.

At the National Research Council, the initial PCR amplification was carried out in a 25-µL reaction volume comprising 5 µL Taq 5X Master Mix (New England Biolabs) 10 µM (0.4 µL) of each forward and reverse primer, 1 µL of DNA template, and 18.2 µL of H2O. The following

program was used for amplification: 95°C for 5 min for initial melting; 35 cycles of 95°C for 30 seconds, 47°C for 30 seconds, and 72°C for 60 seconds; and 72°C for 7 minutes. The only variation in protocols for the primers is that the rust-specific primers used 50°C for the annealing step and the oomycetes primer pair used 52°C for the annealing step. A secondary PCR was then carried out to add dual indexed barcoded adapters with primers targeting D01 and D02 of the initial PCR products. The PCR was carried out in a 20-µL reaction volume containing 10 µL 2x Kapa HiFi HotStart ReadyMix PCR kit (Kapa Biosystems), 5 µL index primer, and 5 µL PCR template. The PCR cycling parameters were 95°C for 3 minutes for initial melting; 12 cycles of 95°C for 30 seconds, 50°C for 30 seconds, and 72°C for 30 seconds; and 72°C for 10 minutes. After each PCR step (Locus and Indexing) a 0.8x Bead Cleanup was performed and a subset of libraries were visually confirmed on an Agilent Tapestation. The completed libraries were quantified by qubit dsDNA HS and an equal mass of each sample was pooled to make the final sequencing pool for each amplicon. Each pool was also checked on an Agilent Tapestation and then quantified by qPCR using the KAPA Quantification Kit for Illumina. The quantified samples were pooled and prepared following the MiSeq Denature and Dilute for 4 nM Libraries Guide. A final sequencing concentration of 10.5pM with 10% 10.5pM PhiX was targeted and loaded on the MiSeq Sequencer using a 600 cycle (2×301bp) run with dual 10bp indexing.

2.4 Metabarcoding data processing

The Illumina MiSeq sequencing adapters and primers were removed from the raw data using Atria (Chuan et al., 2021) and Cutadapt ver.4.1 (Martin, 2011), respectively. The paired-end reads were then processed using DADA2 ver. 2023.7.0 (Callahan et al., 2016) implemented in QIIME2 ver. 2023.7 (Bolyen et al., 2019) for denoising, chimera detection, and amplicon

sequence variants (ASVs) inference using default parameters without trimming or truncating at a specific position, as the ITS region has high length variance.

Taxonomic assignment was initially performed using the QIIME2 q2featureclassifier Naïve Bayes classifier (Bokulich et al., 2018), trained on the UNITE fungal ITS database (version 10 dynamic) (Abarenkov et al., 2024) with a minimum bootstrap confidence of 70%. This approach provided reliable genus-level identifications but did not consistently resolve taxa to the species level. To improve species-level resolution for all genera except Puccinia, we integrated three complementary methods: QIIME2 Naïve Bayes classification, BLASTn, and alignment-based comparison. A local fungal reference database was constructed by retrieving sequences from NCBI using the query: txid4751[Organism] AND (internal transcribed spacer OR ITS) AND 5.8S NOT "sp." NOT genome NOT metagenome NOT mitochondria NOT environmental NOT clone NOT "complete genome" NOT shotgun. A custom BLAST database containing taxonomic identifiers and accession numbers was generated using makeblastdb, and representative ASVs were queried using blastn with a 97% identity threshold and an E-value cutoff of 0.01. For alignment-based classification, ASV sequences were aligned to UNITE reference sequences using MAFFT v7.526 with the FFT-NS-i algorithm (Katoh & Standley, 2013), and the closest reference sequence was identified using the cophenetic function in the APE R package (Paradis & Schliep, 2019). Species-level assignments followed a hierarchical decision rule: full agreement among all three methods resulted in a confirmed species assignment; if full consensus was not achieved, the alignment-based species call was accepted only when supported by at least one additional method; ASVs lacking such support were not assigned to known species.

Species-level identification of ASVs belonging to the rust fungal genus Puccinia was refined using the Automated Oligonucleotide Design Pipeline (AODP) with an in-house curated rust fungi ITS2 database CR-ITS2-refDB (Chen et al., 2022), which identifies diagnostic nucleotide differences among closely related taxa (Chen et al., 2022; Zahariev et al., 2018). A detailed protocol is available at https://bitbucket.org/wenchen_aafc/metabarcoding_rust_fungi. To assess assignment accuracy, representative ASV sequences and reference sequences from the target species and closely related taxa were aligned using MAFFT v7.407 (Katoh & Standley, 2013), followed by approximate maximum-likelihood tree reconstruction in IQ-TREE v3.0.1 (Wong et al., 2025). Phylogenetic trees were visualized in iTOL v.7.5.1 (Letunic & Bork, 2024). ASVs were assigned biotroph status and annotated as plant pathogens via FUNGuildR package (Nguyen et al., 2016). ASVs identified as "plant pathogen" with confidence rankings of "highly probable", "probable," or "possible" are all included as part of the phytopathobiome.

2.5 Statistical analysis and machine learning

All statistical analyses were performed in R (ver. 4.5.1) (Team, 2025). To evaluate site-level environmental variation, Partial Least Squares Discriminant Analysis (PLS-DA) was conducted as a dimensionality-reduction analysis. For each genus of interest, relative abundance within the fungal community and detection frequency across samples and sites were calculated. General linear mixed-effects models (GLMMs) were implemented via the *glmmTMB* (which is able to handle skewed data with random effects) function in glmmTMB package (v1.1.12) (Brooks et al., 2017), to evaluate the effects of site and year, and their interactions on genus-level and species-level rclr-transformed abundances. Site and year were treated as fixed effects, week as a random effect, and repeated measures were nested within year-week as a random effect to account for repeated measures within the same sampling site. To account for unbalanced

sampling across years (resulting from field sites established at different timepoints between 2020 and 2023) post hoc comparisons were performed using the emmeans package (v1.10.2) (Lenth, 2017) with Sidak-adjusted P-values.

Random Forest (RF) modelling using the *randomForest* package (v4.7-1.1) (Liaw & Wiener, 2002) was carried out as an exploratory non-parametric feature selection tool to examine non-linear environmental and landscape associations with pathogen abundance. Because observations were collected repeatedly within sampling sites, the random forest assumption of sample independence was not fully met. Out-of-bag estimates were therefore treated as descriptive measures of model fit and may be optimistic; they were not interpreted as independent validation. Continuous abundances of frequently detected species (*Parastagonospora nodorum*, *Fusarium tricinctum*, *Blumeria graminis*) were analyzed using regression random forest models. Predictor variables included landscape composition (proportions of cereal crops and grasslands at 1–5 km scales) and environmental variables (mean temperature, total precipitation over 7 days, relative humidity, wind speed, and wind direction). Descriptive model fit was summarized using Out-of-Bag (OOB) mean squared error (MSE) and percentage variance explained (R^2). Variable importance was assessed via %IncMSE (percent increase in mean squared error) and IncNodePurity (increase in node purity). These importance measures were interpreted as exploratory associations rather than causal effects. Additionally, generalized linear models were fitted using rclr-transformed genus abundances as responses and top-ranked variables from Random Forests as predictors. The GLMMs and Random Forests served complementary purposes: the GLMMs evaluated site and year effects using the random-effects structure described above, whereas the Random Forests explored non-linear associations with climate and landscape variables. The Random Forest models did not explicitly account for

within-site temporal autocorrelation, so their performance and variable-importance rankings were interpreted cautiously.

2.6 Data and coding availability

All raw sequencing data were submitted to the NCBI Sequence Read Archive (SRA) under BioProject accession PRJNA1469275. Due to the large volume of the sequencing dataset, BioSample accessions will become available once the SRA staff has completed the review process (review still in progress as of May 21, 2026). All code and scripts for this project are available at https://github.com/WenChenAAFC/biovigilance_morgan

3. Results

3.1 Weather and land use conditions at sampling sites

Total cereal coverage across sites ranged from 0.03–85.9% within the 1-km buffer and from 0.7–44.4% within the 5-km buffer (supplementary Figure S1). At the 5-km scale, cereal coverage was highest at the SK and AB sites (>25%) and lowest at the ON site (~1%). Cereal crop composition was the dominant factor distinguishing sites, with higher proportions of wheat, barley, and corn driving clear between-site separation in multivariate space (Figure 2A). Specifically, SK01, MB01, and AB09 were characterized by high spring wheat coverage, with AB09 also showing substantial barley production, whereas BC10, QC07, and NS01 were dominated by corn.

Seasonal variation of weather conditions at each site is given in supplementary Figure S2. Temperature is higher in the middle of the sampling season. Sites AB09, SK01, and MB01 are at a higher altitude than the other sites and therefore have lower overall pressure. Precipitation and humidity is higher at the end of the sampling season. Wind speed emerged as the most influential weather variable shaping site-level differences (Figure 2A), with consistently higher values at SK01, MB01, and AB09 (supplementary Figure S1). In contrast, seasonal patterns were driven primarily by weather conditions, as shifts in temperature, wind direction, wind speed, humidity, and precipitation aligned strongly with within-site temporal variation across sampling periods (Figure 2B; supplementary Figure S2; supplementary Figure S3).

3.2 Summary of sequencing data and overall community

The final ASV abundance table for the fungal communities contained over 14.4 million high-quality reads, with an average of 32,933 ± 37,756 reads per sample. Across all samples,

4,650 ASVs were identified, spanning substantial taxonomic diversity, including 8 phyla, 32 classes, 124 orders, 364 families, and 967 genera. Across all sites and years, the airborne fungal communities were dominated by Ascomycota and Basidiomycota, which accounted for 83.9% and 15.8% of total sequence abundance, respectively. Minor phyla included Entomophthoromycota (0.14%), Mucoromycota (0.14%), Mortierellomycota ($2.67 \times 10^{-2} \pm 2.91 \times 10^{-4}$%), Chytridiomycota ($6.81 \times 10^{-3} \pm 6.85 \times 10^{-5}$%), Neocallimastigomycota ($3.76 \times 10^{-4} \pm 2.54 \times 10^{-5}$%), and Basidiobolomycota ($1.67 \times 10^{-4} \pm 1.13 \times 10^{-5}$%). At the genus level, the communities were primarily composed of *Cladosporium* (55.30 ± 21.57%), *Alternaria* (19.35 ± 15.69%), and *Stemphylium* (4.30 ± 12.88%) (supplementary Figure S4).

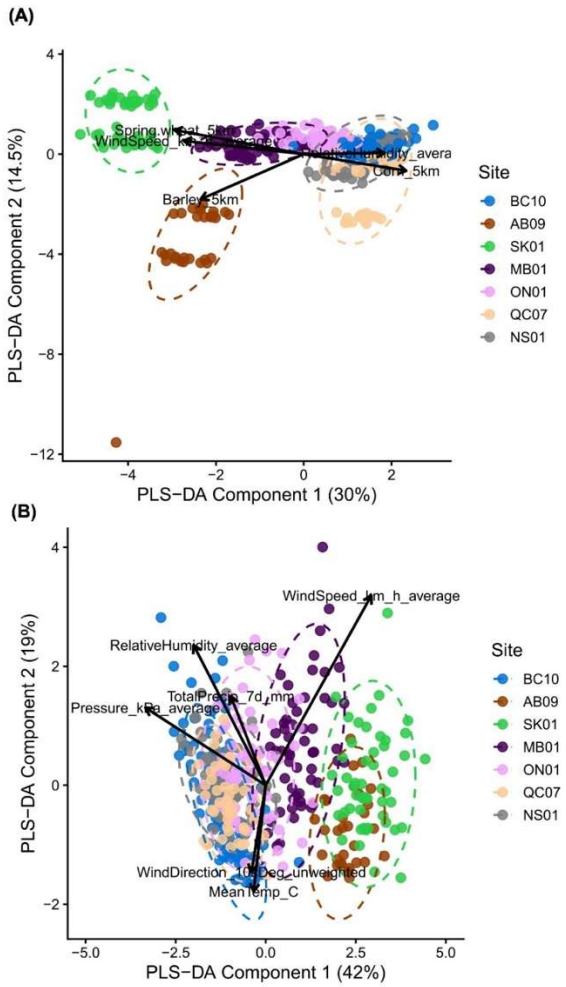

Figure 2. Partial least squares discriminant analysis (PLS-DA) of site-level environmental profiles. (**A**) Model including crop composition and key weather variables. (**B**) Model including only meteorological predictors. Ellipses represent 95% confidence intervals for each site, and vectors indicate variables contributing most strongly to separation along Components 1 and 2.

FUNGuild (Nguyen et al., 2016) identified 1649 ASVs (35.44% of total ASVs) as potential phytopathogens (patho-ASVs). These patho-ASVs contained 12,354,433 reads (86.04% of total reads) with an average of 28,335.86±33,234.8 reads per sample. This suggest that a smaller proportion of the patho-ASVs contained majority of the recovered metabarcodes, demonstrating that the phytopathogens are more abundant in the biome. The phytopathobiome compassed four (4) phyla, 19 classes, 58 orders, 149 families, and 311 genera that were

identified as possible, probably, or highly probably phytopathogens. The pathogenic fungal communities were composed of Ascomycota (94.3±0.14%), Basidiomycota (5.73±1.19E-02%), Chytridiomycota (6.13E-03±7.39E-05%), and Mucoromycoda (2.95E-03±6.97E-05%). The most abundant genera containing potential pathogens identified included *Cladosporium* (56.4%), *Alternaria* (20.9%), and *Stemphylium* (4.56%) (supplementary Figure S4).

Of the 12 targeted cereal-associated fungal pathogen genera, 10 were detected across all samples (supplementary Figure S5), comprising a total of 133 ASVs, whereas *Pyrenophora* and *Rhynchosporium* were absent. The combined relative abundance of these 10 genera ranged from 0 to 76.7% across samples, with an overall mean of 1.64%. The most abundant genera across sites were *Claviceps*, *Parastagonospora*, and *Ustilago*, while *Tilletia* and *Zymoseptoria* were consistently low (supplementary Figure S5A). *Parastagonospora* and *Ustilago* had the highest detection across samples, whereas *Tilletia* and *Zymoseptoria* were the least frequently detected (supplementary Figure S5B). Site-level dominance patterns were strongly genus-specific: BC10 had the highest abundance of *Claviceps* and *Leptosphaeria*; AB09 and SK01 of *Parastagonospora* and *Ustilago*; MB01 of *Claviceps*, *Ustilago*, and *Parastagonospora*; ON01 of *Puccinia*, *Ustilago*, and *Bipolaris*; QC07 of *Fusarium* and *Blumeria*; and NS01 of *Blumeria* (supplementary Figure S6).

3.3 The cereal crop phytopathobiome

3.3.1 *Parastagonospora nodorum*

Among the eight ASVs assigned to *Parastagonospora*, three were identified as *P. nodorum*, the causal agent of Stagonospora nodorum blotch (SNB), representing on average 0.25% of total fungal communities (Table 1). *P. nodorum* was detected frequently at Prairie sites, occuring in

67.6–78.9% of samples at AB09, SK01, and MB01, but appeared far less often at coastal and eastern locations. Relative abundance was likewise highest in the Prairies, particularly in 2023, indicating strong spatial structuring (Figure 3A). Seasonally, abundance consistently peaked in June and July across Prairie provinces, aligning with wheat heading and early grain filling. Interannual variation was most pronounced at AB09, pointing to additional year-specific environmental influences.

Random forest modelling identified spring wheat as the highest-ranked predictor of *P. nodorum* abundance, consistent with the prevalence of wheat in Prairie landscapes (Figure 3B). This relationship was further supported by a strong positive correlation between abundance and spring wheat coverage (Spearman's $r = 0.62$, $P < 0.001$, supplementary Figure S7), providing empirical support for the spatial hypothesis. Abundance peaks in June at Prairie sites coincides with rising temperatures, frequent rainfall events, and long dew periods, creating ideal conditions for *P. nodorum* infection and spread (Figure 3B).

Table 1. Identified cereal-associated fungal pathogen species/species complexes, their relative abundance across all samples and associated disease.

Genus	Species	Species complex	Relative Abundance (%, mean ±sd)	Notes
Parastagonospora	*Parastagonospora nodorum*	—	0.2524±0.6859	Causal agent of Stagonospora nodorum blotch (SNB), wheat
Bipolaris	*Bipolaris zeicola*	—	0.0004±0.0055	Cause of Northern Corn Leaf Spot Disease
Blumeria	*Blumeria graminis*	—	0.0709±0.4023	Cause of powdery mildew on several cereal types.
Fusarium	*Fusarium poae*	—	0.0008±0.0088	Cause of FHB on wheat, barley and oats
Fusarium	*Fusarium sambucinum*	—	0.0017±0.0268	Fusarium head blight and root/crown rot of cereals
Tilletia	*Tilletia indica*	—	0.0012±0.0146	Causal agent of Karnal bunt of wheat
Ustilago	*Ustilago maydis*	—	0.0679±0.3865	Causes corn smut on maize

Ustilago	*Ustilago hordei*	—	0.0499±0.3751	Causes covered smut of barley
Ustilago	*Ustilago coicis*	—	0.0214±0.1196	Smut of Job's tear millet
Ustilago	*Ustilago kummeri*	—	0.0033±0.0275	closely related to cereal smut pathogens
Puccinia	*Puccinia coronata*	Puccinia_coronata.VARavenaeFSPavenae	0.0199±0.11522	Crown rust of oats
Puccinia	*Puccinia coronata*	Puccinia_coronata.VARcoronata	0.0086±0.0889	Infects cereals + grasses
Puccinia	*Puccinia coronata*	Puccinia_coronati.hordei	0.0019±0.0156	Crown rust of barley
Puccinia	*Puccinia graminis*	Puccinia_graminis.CladeII	0.0015±0.02325	stem rust
Puccinia	*Puccinia graminis*	Puccinia_graminis.CladeIII	0.0136±0.0693	stem rust
Puccinia	*Puccinia hordei*	Puccinia_hordei.CladeI	0.00001±0.00012	barley leaf rust
Puccinia	*Puccinia hordei*	Puccinia_hordei.CladeII	0.003±0.0322	barley leaf rust

	Puccinia	Puccinia_recondita.CladeI		
Puccinia	*recondita*	V	0.003±0.0321	Leaf rust
	Puccinia	Puccinia_recondita.CladeV		
Puccinia	*recondita*	I	0.0101±0.06614	Leaf rust

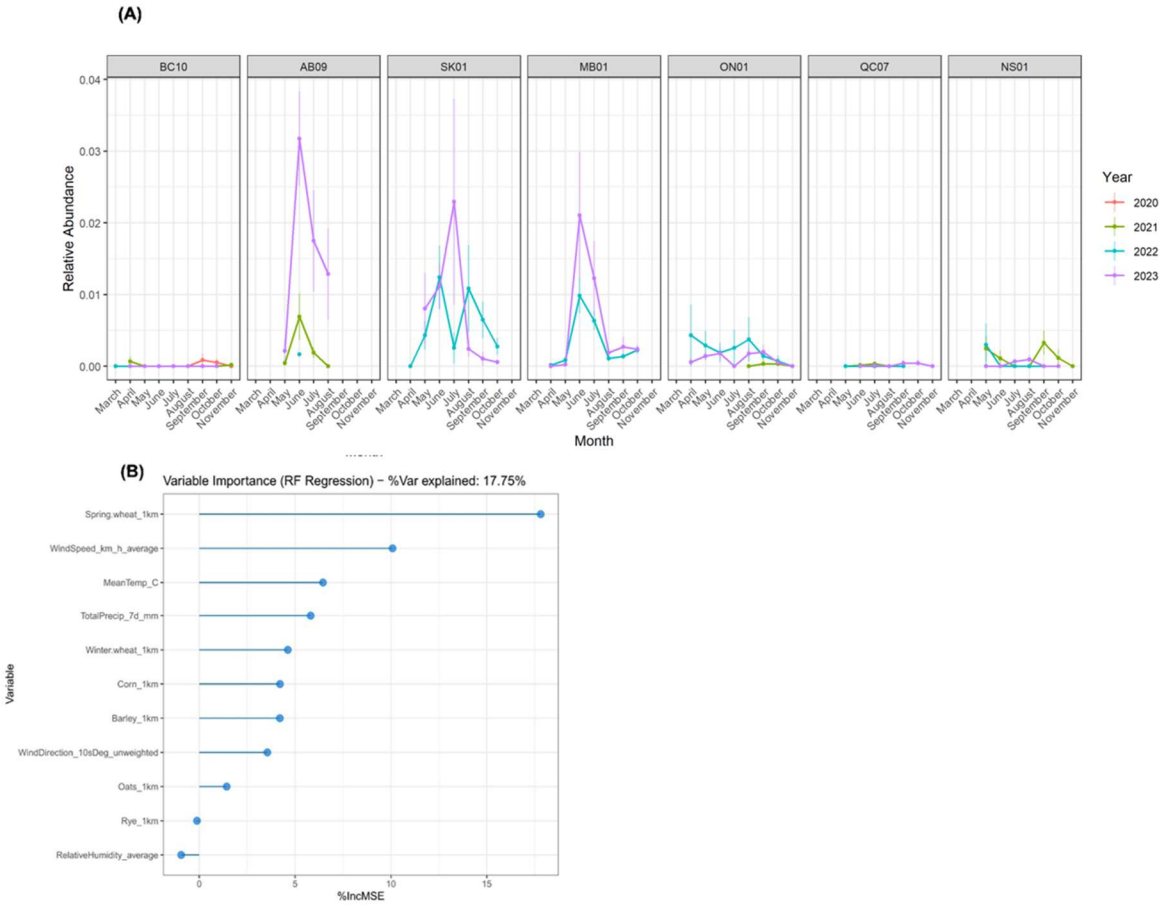

Figure 3. Seasonal patterns and environmental drivers of *Parastagonospora nodorum* in aerobiological surveillance across Canada. (**A**) Relative abundance of *P. nodorum* detected at seven sentinel sites (2020–2023); error bars indicate the standard error of monthly means. (**B**) Variable importance from a Random Forest regression model (% variance explained = 17.75), summarizing the relative contribution of crop distributions and meteorological variables to observed abundance patterns.

3.3.2 *Ustilago* species

Ustilago was widely distributed across the study region, exhibiting both high detection frequency and substantial relative abundance at several sites. It was detected in more than 30% of all samples, indicating a persistent airborne presence throughout the growing season (supplementary Figure S5B). Detection frequencies were highest at Prairie sites, particularly MB01, where *Ustilago* was detected in up to 91.2% of samples, while coastal and eastern sites showed lower but consistent occurrence (supplementary Figure S5B). Relative abundance was generally

elevated at MB01, AB09, SK01, and ON01, highlighting strong regional structuring linked to cereal-producing areas (supplementary Figure S6). A total of 23 *Ustilago* ASVs were detected across the study period. Of these, three to *U. hordei*, two each to and *U. coicis* and *U. kummeri*, and one to *U. maydis*, which were cereal-associated pathogens (Table 1). Different *Ustilago* species showed distinct spatial and seasonal patterns (Figure 4). *U. maydis* (corn smut) was detected mainly at ON01, with a detection frequency of 46%, particularly at the beginning and end of the growing season, consistent with local maize production (Figure 4A, supplementary Figure S8). *U. hordei* (covered smut of barley) was most abundant at AB09 and SK01, where barley proportions were highest (Figure 4B). *U. coicis* was observed at all sites except BC10, indicating a broader distribution across regions (Figure 4C).

While the genus *Ustilago* was widely distributed, resolving it to the species level revealed distinct host-specific spatial patterns (e.g., *U. maydis* in corn-heavy Ontario vs. *U. hordei* in barley-heavy Prairies), providing evidence for the taxonomic resolution hypothesis.

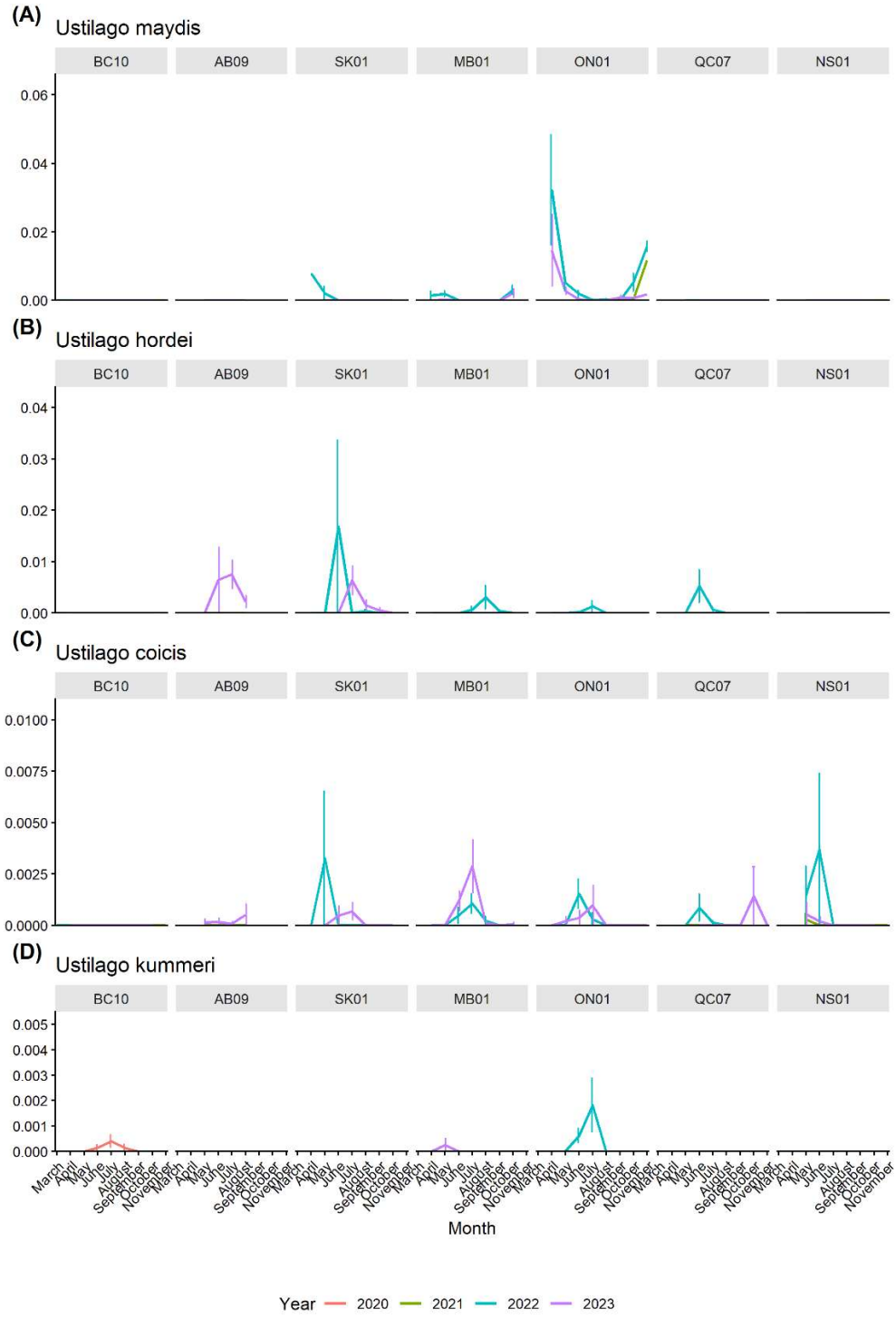

Figure 4. Seasonal dynamics of four cereal associated *Ustilago* species detected at seven sentinel sites (2020–2023). Panels show monthly mean relative abundances for (**A**) *U. maydis*, (**B**) *U. hordei*, (**C**) *U. coicis*, and (**D**) *U. kummeri* across all sampling years. Error bars indicate the standard error of monthly means.

3.3.3 *Fusarium* species

Fusarium was consistently detected across all sampling sites and years, exhibiting moderate to high detection frequencies (17.6–45.6%) and relatively stable spatial distribution (Figure 5A, supplementary Figure S5). Detection frequencies were highest at MB01, ON01, QC07, and SK01, indicating widespread and persistent airborne presence across both Prairie and eastern regions. Relative abundance varied among sites, with pronounced peaks at MB01 and QC07, highlighting localized hotspots of *Fusarium* enrichment. Strong interannual variability characterized *Fusarium* dynamics. Overall abundance was significantly higher in 2022 and 2023 compared to 2020 and 2021 ($P < 0.001$). Seasonally, *Fusarium* abundance tended to increase during spring and early summer, with notable peaks observed in April 2022 at MB01 and in July–August 2023 at QC07 (Figure 5A). Random forest modelling ranked relative humidity as the highest-ranked climatic predictor of *Fusarium* abundance, while the mixed-effects model found an association with relative humidity ($P < 0.001$), a pattern that aligns with the temporal hypothesis, but this observational association does not establish a regulatory mechanism for airborne inoculum survival and dispersal (Figure 5B). Random forest analysis further indicated that several crop and vegetation types, including spring wheat, barley, grassland, and corn, were highly ranked predictors of *Fusarium* dynamics (Figure 5B).

A total of nineteen *Fusarium* ASVs were detected; however, most ASVs cannot be identified at species level, only 2 ASVs were identified as cereal-associated pathogenic species as *F. poae*, and *F. sambucinum,* separately, with very low abundance (Table 1).

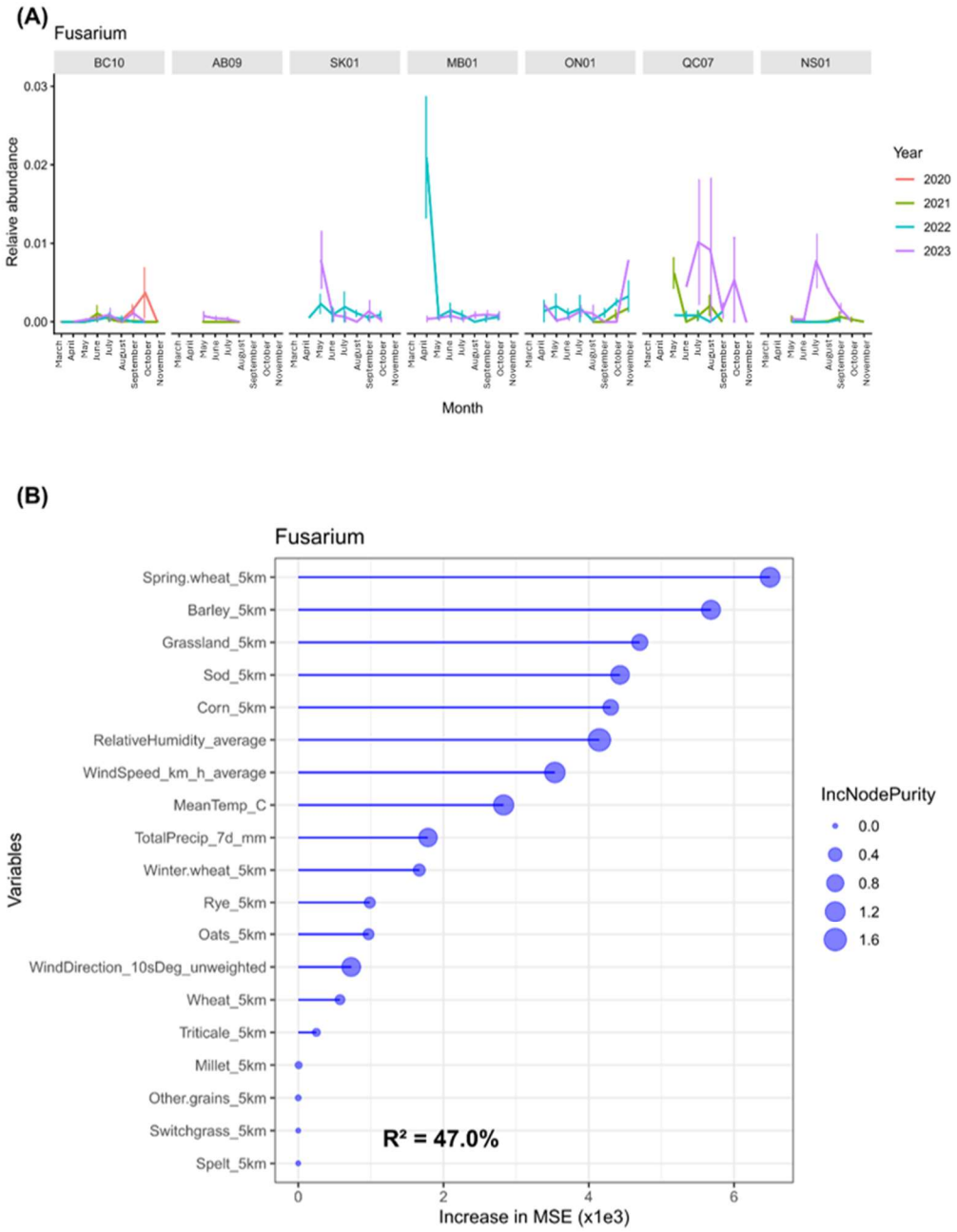

Figure 5. Seasonal dynamics of *Fusarium* detected at seven sentinel sites from 2020 to 2023(A). (B) Important environmental variables and host-related variables associated with *Fusarium* abundance, as determined by random forest regression modelling.

3.3.4 *Puccinia* species

A total of 40 *Puccinia* ASVs were detected, of which 35 were assigned to 18 identified species or formae speciales using AODP, including nine cereal-associated pathogens (Table 1). The most abundant species included *Puccinia recondita*, *P. coronata*, and *P. hordei*, all of which are major rust pathogens of cereal crops. *Puccinia* species were intermittently detected across sampling sites, exhibiting generally low detection frequencies but clear spatial and temporal patterns (supplementary Figure S9). Detection frequency varied among species, with *Puccinia graminis* (Clade III), *P. coronata* (var. avenae f. sp. avenae), and *P. recondita* (Clade VI) (supplementary Figure S10) showing relatively higher occurrence across multiple sites, particularly at ON01 and BC10. In contrast, other taxa, including *P. hordei* and *P. graminis* (Clade II), were detected less frequently and displayed more restricted distributions.

Temporal dynamics of *Puccinia* species were characterized by sporadic but pronounced peaks in relative abundance, rather than consistent seasonal trends (Figure 6). Several species exhibited sharp, transient increases during mid- to late growing season. For example, *P. graminis* (Clade III) and *P. coronata* (var. avenae f. sp. avenae) showed notable peaks in 2023, particularly at ON01 and QC07, while *P. recondita* (Clade VI) displayed episodic increases across multiple sites, with higher abundance observed in 2022 and 2023. Species associated with barley and oat rusts, including *P. coronata* and *P. hordei*, showed localized abundance peaks, suggesting site-specific host or environmental conditions influencing their occurrence. In contrast, *P. graminis*, a pathogen with a broader host range, exhibited wider spatial distribution and more frequent detection across sites.

The use of the AODP pipeline to resolve *Puccinia* to species and clade levels allowed for the detection of host-specific patterns that would have remained cryptic at the genus level, further supporting the taxonomic resolution hypothesis.

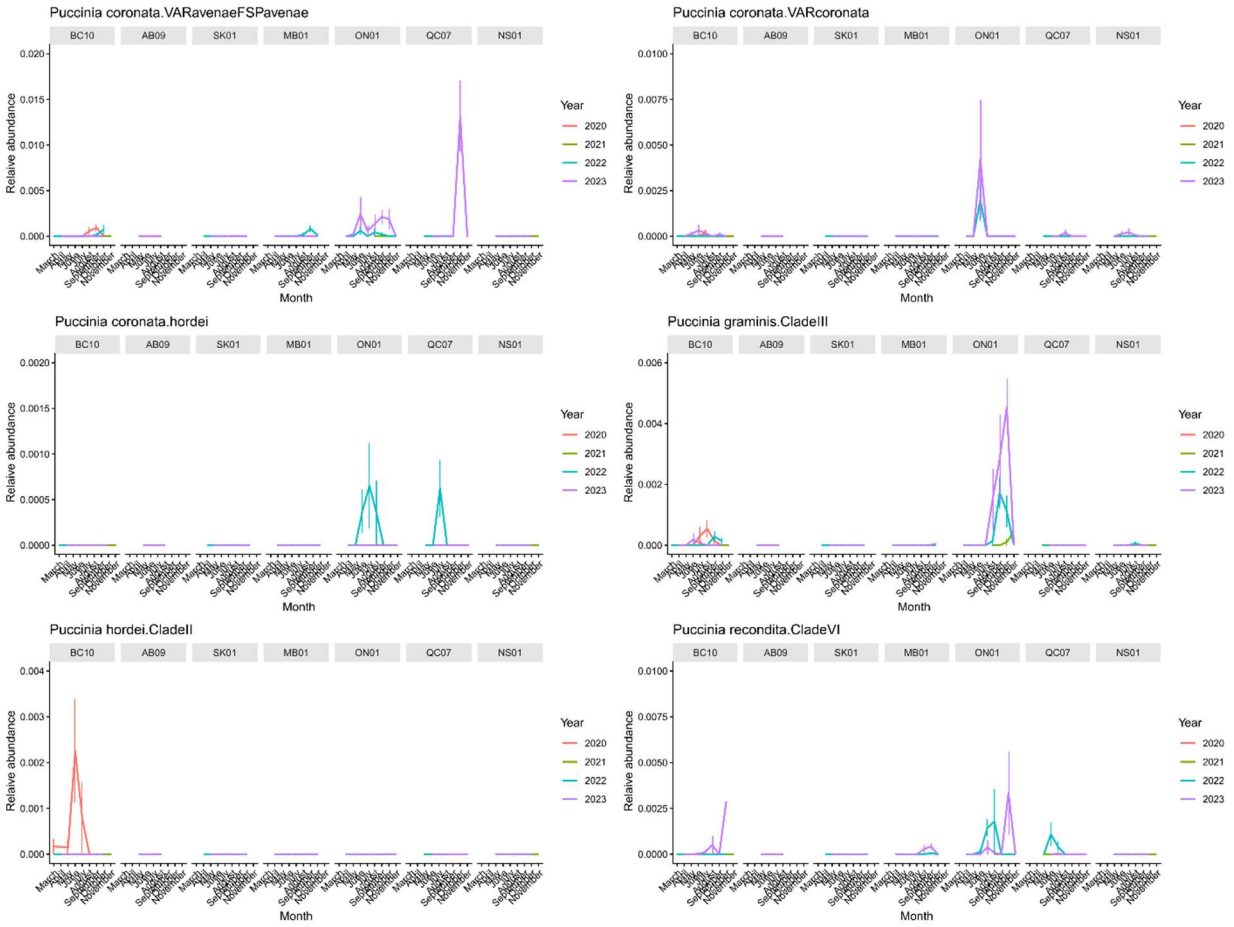

Figure 6. Seasonal dynamics of cereal-associated *Puccinia* species complex detected at seven sentinel sites (2020–2023). Error bars represent the standard error of monthly means.

Overall, *Puccinia* dynamics were characterized by low baseline abundance punctuated by episodic outbreaks, with substantial interannual variability and site-specific patterns. These observations suggest that airborne *Puccinia* populations are influenced by localized host availability and episodic environmental conditions favorable for spore release and dispersal.

3.3.5 *Blumeria graminis*

Seven *Blumeria* ASVs were detected across the dataset, and all were identified as *Blumeria graminis*, the causal agent of powdery mildew on cereals and an economically important

pathogen worldwide (Inuma et al., 2007). *B. graminis* occurred at every sampling site, with pronounced seasonal peaks (Figure 7A). Notably high abundances were observed at NS01 during May–June 2021 and at QC07 in October 2023, reflecting strong temporal and regional variation in airborne inoculum (Figure 7B).

Random forest analysis highlighted several key climatic and host-related predictors associated with *B. graminis* abundance (Figure 7B). Relative humidity emerged as the highest-ranked environmental predictor, followed by the local presence of winter wheat, barley, and corn within a 5km radius. These variables collectively contributed most to model performance, suggesting that moisture conditions and host-crop distribution were associated with airborne patterns of *B. graminis* across the surveillance network.

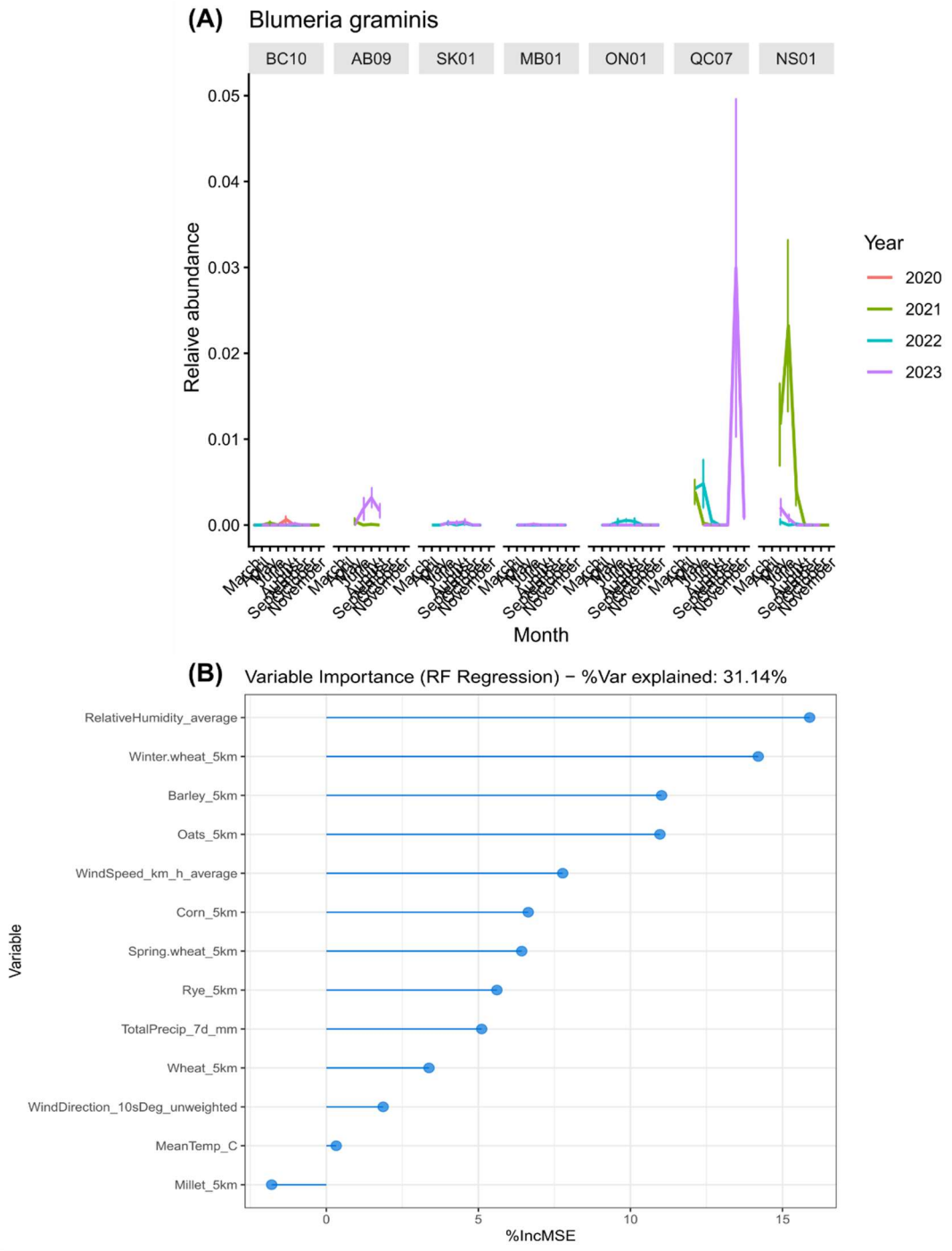

Figure 7. Seasonal patterns and environmental drivers of *Blumeria graminis* in aerobiological surveillance across Canada. (**A**) Relative abundance of *B. graminis* detected at seven sentinel sites (2020–2023); error bars indicate the standard error of monthly means. (**B**) Variable importance from a Random Forest regression model (% variance explained = 17.75), summarizing the relative contribution of crop distributions and meteorological variables to observed abundance patterns.

4. Discussion

This study demonstrates that airborne cereal-associated fungal communities across Canadian agroecosystems are structured by a hierarchical interaction between host availability and atmospheric processes. Landscape composition constrains the pool of potential inoculum, while meteorological conditions regulate its release, dispersal, and temporal expression. This dual-filtering framework helps reconcile previously fragmented observations in aerobiological studies and provides a mechanistic basis for understanding spatial and temporal variation in airborne plant pathogens. Importantly, the strength of these drivers varies among taxa, producing distinct patterns at both the genus and species levels.

4.1 Host preference as a driver of spatial dynamics in airborne cereal-associated pathogen communities

In strong support of the spatial hypothesis, landscape composition emerged as a key determinant of the spatial distribution and abundance of airborne plant pathogens, largely mediated by host specificity (Mahas et al., 2026; Moore & Borer, 2012). Pathogens with narrow host ranges showed strong spatial coupling with the respective dominant crops, whereas generalist displayed broader distributions shaped by a combination of host diversity and environmental conditions. These patterns are consistent with ecological theory predicting tighter resource coupling for specialists and greater environmental responsiveness among generalists.

Wheat-associated pathogens, particularly *Parastagonospora*, were most abundant at Prairie sites with extensive spring wheat coverage. *P. nodorum*, the dominant species in this genus, causes Septoria nodorum blotch which reduces photosynthetic capacity, grain quality, and total yield (Cowger et al., 2020; Downie et al., 2021; Hafez et al., 2020). The alignment between

P. nodorum abundance and wheat phenology highlights the predictability of dispersal patterns for host-specialized pathogens. The high abundance of *P. nodorum* in the prairies is also shown in the Canadian Plant Disease Survey (Elmhirst, 2023).

Smut fungi (*Ustilago* spp.) showed similarly strong host associations but with greater heterogeneity at the species level. While the genus was widely distributed, individual species exhibited distinct spatial patterns reflecting their specific hosts. For example, *U. maydis*, specialized on corn (Brefort et al., 2009; Kahmann & Kämper, 2004), was concentrated at ON01 dominated by corn, whereas *U. hordei* was associated with barley-rich landscapes, demonstrating how host-restricted pathogens track specific cereal distributions within mixed agricultural landscapes (Cheng et al., 2026; Gaudet et al., 2010). These findings highlight an important methodological implication: genus-level aggregation can obscure ecologically meaningful patterns, particularly for taxa with strong intra-genus differences in host specificity.

In contrast, *Fusarium* showed broad spatial distributions, consistent with its wide host range, ability to colonize both cultivated cereals and wild grasses, and persistence on crop residues (Goswami & Kistler, 2004; Harris et al., 2016; Wu et al., 2024). These ecological traits, combined with inputs from diverse vegetation types documented in this study, help explain *Fusarium*'s widespread airborne presence across agricultural landscapes. A key limitation is the inherently poor species-level resolution of *Fusarium* when using ITS2. Most ASVs could not be classified beyond the genus, reflecting well-documented challenges in resolving Hypocreales with this marker, where multiple distinct species often collapse into a single UNITE species (Cobo-Díaz et al., 2019; Lücking et al., 2020). Species-level identification, particularly for pathogenic taxa, typically requires higher-resolution markers such as EF1-α or targeted qPCR assays . As a result, our interpretations necessarily remain at the genus level, and future

surveillance efforts will benefit from integrating metabarcoding with species-specific molecular diagnostics.

Blumeria graminis is an obligate biotrophic powdery mildew infecting cereal crops within the subfamily *Pooideae*, including wheat, barley, rye, and oats (Inuma et al., 2007; Mapuranga et al., 2022b). All detected *Blumeria* ASVs were assigned to the species level but could not be resolved into formae speciales due to limitations of ITS metabarcoding. Despite this, pronounced spatial and temporal peaks indicate that airborne metabarcoding can still capture meaningful landscape-level patterns for obligate biotrophs. These peaks likely reflect localized host availability combined with favorable environmental conditions for conidial production and dispersal.

Puccinia is the largest rust genus with over 4,000 described species (Avasthi et al., 2023). In contrast to other genera, *Puccinia* exhibited high taxonomic resolution in this study, enabling species- and clade-level insights, due to the application of AODP classification method. The detection of multiple cereal-associated rust species, including *P. coronata*, *P. graminis*, and *P. recondita*, revealed strong site-specific patterns, with the highest abundance observed at ON01. The co-occurrence of multiple clades at this site suggests that it may function as a regional receptor, integrating both local and long-distance inoculum. This highlights the importance of considering atmospheric transport processes alongside local host availability when interpreting rust dynamics.

Collectively, these results demonstrate that host preference is a fundamental driver of spatial structuring in airborne pathogen communities, with its influence most pronounced in host-specialized taxa. Importantly, these findings confirm the taxonomic resolution hypothesis by demonstrating that genus-level aggregation can obscure ecologically meaningful patterns,

particularly for taxa with high intra-genus variability in host specificity, underscoring the importance of species-level resolution for accurately linking airborne dynamics to agricultural landscapes.

4.2 Environmental drivers of airborne cereal-associated pathogen communities

As predicted by the temporal hypothesis, temporal dynamics across pathogen taxa were primarily governed by seasonal climatic forcing, which determined the timing, magnitude, and persistence of airborne abundance. Two dominant modes of temporal behavior emerged: (i) phenology-constrained peaks in host-specialized pathogens, and (ii) climate-responsive persistence in generalist taxa.

Host-specialized pathogens exhibited temporally predictable peaks closely aligned with crop development stages. *Parastagonospora nodorum* consistently peaked during early to mid-summer, coinciding with wheat heading and grain filling. This timing reflects the pathogen's infection biology, where sporulation on senescing tissues and favorable warm, humid conditions promote rapid inoculum production (Downie et al., 2021; Pilo et al., 2022). Similarly, *Blumeria graminis* showed pronounced but episodic peaks, reflecting its dependence on both susceptible hosts and narrow climatic windows suitable for conidial development (Cao et al., 2012). Powdery mildew development is optimal at temperatures between 15 and 22 °C, while infection efficiency and disease progression decline sharply above 25 °C (Mathre, 1997). In these taxa, meteorological conditions primarily modulated the intensity of host-driven seasonal patterns rather than determining their timing.

In contrast, generalist taxa such as *Fusarium* exhibited broader temporal windows and greater sensitivity to environmental variability. Continuous detection across the growing season

indicates sustained inoculum availability, supported by multiple host reservoirs and saprophytic survival on crop residues (Karlsson et al., 2021; Marzec-Schmidt et al., 2021). Elevated abundance during periods of high humidity and precipitation highlights the importance of atmospheric conditions in regulating spore maturation, release, and dispersal (Grinn-Gofroń & Bosiacka, 2015; Manstretta & Rossi, 2015). The pronounced early-season peak observed at MB01 illustrates how local microclimatic conditions and residue-derived inoculum can generate site-specific dynamics even within broader regional patterns (Hoffmann et al., 2023).

Late-season dynamics were particularly evident for *Puccinia* and, in some cases, *Blumeria*. Several *Puccinia* species exhibited sharp, episodic peaks in mid- to late season, rather than continuous presence. These patterns are consistent with the epidemiology of rust fungi, where repeated cycles of urediniospore production and long-distance dispersal lead to regional accumulation of inoculum over time (Meyer et al., 2017; Prank et al., 2019). The importance of wind speed and humidity in shaping these dynamics underscores the role of atmospheric transport and environmental suitability in driving temporal variability (Aylor, 2003). The episodic nature of *Puccinia* abundance suggests that regional-scale dispersal events may dominate over local inoculum production, particularly for pathogens capable of long-distance movement.

Overall, these findings demonstrate that temporal dynamics in airborne pathogen communities emerge from the interaction between environmental suitability and host availability. Climatic factors regulate spore release, survival, and dispersal, while host phenology constrains when inoculum can be produced. This interaction results in sharply defined, phenology-driven peaks for specialists and broader, climate-sensitive patterns for generalists, providing a unified explanation for the diverse temporal behaviors observed across taxa.

4.3 Integrating airborne monitoring and disease management

Airborne metabarcoding provides a high-resolution tool for capturing pathogen presence across landscapes, including both dominant and cryptic taxa. When combined with climatic and landscape data, airborne inoculum information has been shown to improve epidemiological understanding and inform proactive disease management by identifying when and where airborne inoculum levels are high and by helping refine disease warning systems (Chen et al., 2024; Chen et al., 2022; Reich et al., 2023; Van der Heyden et al., 2021).

The clear phenology-aligned peaks observed for *P. nodorum* and the late-season accumulation patterns in *Puccinia* species demonstrate that airborne monitoring can resolve pathogen-specific risk windows across regions. Such information has direct applications for disease management, particularly for optimizing the timing of interventions such as fungicide applications (Van der Heyden et al., 2021). For pathogens with well-defined infection windows, such as *Fusarium* species causing head blight and rust fungi (*Puccinia* spp.), integrating airborne inoculum data with meteorological conditions and host phenology can enhance forecasting accuracy and enable more precise, targeted disease management (Prank et al., 2019; Van der Heyden et al., 2021; West et al., 2017).

Moreover, the strong regional differences observed in pathogen composition and dynamics suggest that region-specific surveillance networks may be necessary to capture spatial heterogeneity in disease risk across diverse agroecosystems. Even taxa with low or sporadic detection, such as *Tilletia* or *Zymoseptoria*, may have epidemiological significance if their presence coincides with susceptible host stages or facilitates long-distance dispersal (Carris et al., 2006; Francisco et al., 2019; McDonald et al., 2022; Seethapathy, 2025).

5. Conclusions and Future Work

5.1 Conclusions

This study provides a comprehensive characterization of the airborne phytopathobiome across Canada's major agricultural landscapes, demonstrating that fungal communities are governed by a hierarchical interaction between host availability and atmospheric processes. By integrating nationwide aerobiological monitoring with ITS2 metabarcoding and high-resolution ancillary metadata, this research successfully validated the following three hypotheses:

- **Validation of the Spatial Hypothesis:** Landscape composition emerged as the primary determinant of spatial structuring. Pathogens with narrow host ranges, such as the wheat specialist *Parastagonospora nodorum* and host-specific *Ustilago* species, exhibited distributions strictly coupled with the prevalence of their respective host crops. In contrast, generalist taxa like *Fusarium* and *Blumeria graminis* displayed broader spatial distributions reflecting their wider ecological versatility.
- **Validation of the Temporal Hypothesis:** Seasonal dynamics across pathogen taxa were regulated by climatic forcing and host phenology. For host-specialists, abundance peaks aligned precisely with critical crop development stages, such as wheat heading for *P. nodorum*. For more generalist or long-distance dispersing taxa like *Fusarium* and *Puccinia*, relative humidity and wind speed emerged as dominant environmental drivers, modulating spore release and dispersal throughout the growing season.
- **Validation of the Taxonomic Resolution Hypothesis:** This study underscores the critical importance of species-level identification in aerobiological surveillance. By utilizing advanced bioinformatic tools like the AODP pipeline, we resolved host-specific

patterns within complex genera—such as the differentiation between corn-specialized *U. maydis* and barley-associated *U. hordei*—that would have remained cryptic at the genus level.

Overall, this work establishes that combining airborne metabarcoding with landscape and climatic data provides a robust, scalable framework for modern biovigilance. These insights allow for the identification of high-risk periods and locations, supporting a shift from reactive disease management toward proactive, evidence-based interventions.

5.2 Future Work

While this research provides a strong foundation for a nationwide biovigilance toolbox, several avenues for future work remain:

1. **Bridging Inoculum to Infection:** Airborne DNA detection currently represents inoculum pressure rather than realized field infection. Future research should aim to establish quantitative relationships between airborne signals and actual disease outcomes to improve the utility of these data for on-farm decision-making.
2. **Refining Environmental Models:** Current datasets may not capture fine-scale microclimatic variability within crop canopies. Incorporating high-resolution, field-level microclimatic measurements would enhance the accuracy of predictive models. Including farm practices (ex: tillage, crop rotation, pesticide usage) would further refine these predictive models. Because the Random Forest models did not explicitly represent repeated observations within sites, their out-of-bag performance and variable-importance rankings should be regarded as exploratory.

3. **Expanding Taxonomic Resolution:** While high resolution was achieved for *Puccinia*, other significant genera like *Fusarium* remain difficult to resolve with the ITS2 marker. Future surveillance would benefit from multi-marker approaches (e.g., incorporating *EF1α*) and the expansion of curated, host-annotated reference databases.

4. **Operational Forecasting:** Integrating these real-time monitoring data streams into predictive modelling frameworks is a critical next step. Developing operational disease forecasting systems will enable the timely, proactive management required to ensure the long-term sustainability of Canadian cereal production.

Statement on the use of Generative AI

GPT-4o and Google Gemini were both used to assist in this work. It was used for three purposes: explaining error messages when writing code, writing regex for pattern matching, and correcting sentence structure and grammar. It was not used to generate the text of this thesis, the figures, or design the methodology.

References

Abarenkov, K., Nilsson, R. H., Larsson, K.-H., Taylor, A. F. S., May, T. W., Frøslev, T. G., Pawlowska, J., Lindahl, B., Põldmaa, K., Truong, C., Vu, D., Hosoya, T., Niskanen, T., Piirmann, T., Ivanov, F., Zirk, A., Peterson, M., Cheeke, T. E., Ishigami, Y., … Kõljalg, U. (2024). The UNITE database for molecular identification and taxonomic communication of fungi and other eukaryotes: Sequences, taxa and classifications reconsidered. *Nucleic Acids Research*, *52*(D1), D791–D797. https://doi.org/10.1093/nar/gkad1039

Altschul, S. F., Gish, W., Miller, W., Myers, E. W., & Lipman, D. J. (1990). Basic local alignment search tool. *Journal of Molecular Biology*, *215*(3), 403–410. https://doi.org/10.1016/S0022-2836(05)80360-2

Avasthi, S., Gautam, A. K., Niranjan, M., Verma, R. K., Karunarathna, S. C., Kumar, A., & Suwannarach, N. (2023). Insights into Diversity, Distribution, and Systematics of Rust Genus Puccinia. *Journal of Fungi*, *9*(6), 639. https://doi.org/10.3390/jof9060639

Aylor, D. E. (1983). Escape of *Peronospora tabacina* Spores from a Field of Diseased Tobacco Plants. *Phytopathology*, *73*(4), 525. https://doi.org/10.1094/Phyto-73-525

Aylor, D. E., Fry, W. E., Mayton, H., & Andrade-Piedra, J. L. (2001). Quantifying the Rate of Release and Escape of *Phytophthora infestans* Sporangia from a Potato Canopy. *Phytopathology®*, *91*(12), 1189–1196. https://doi.org/10.1094/PHYTO.2001.91.12.1189

Aylor, D. E. (2003). Spread of Plant Disease on a Continental Scale: Role of Aerial Dispersal of Pathogens. *Ecology*, *84*(8), 1989–1997. https://doi.org/10.1890/01-0619

Banchi, E., Ametrano, C. G., Stanković, D., Verardo, P., Moretti, O., Gabrielli, F., Lazzarin, S., Borney, M. F., Tassan, F., Tretiach, M., Pallavicini, A., & Muggia, L. (2018). DNA metabarcoding uncovers fungal diversity of mixed airborne samples in Italy. *PLOS ONE*, *13*(3), e0194489. https://doi.org/10.1371/journal.pone.0194489

Bentley, D. R., Balasubramanian, S., Swerdlow, H. P., Smith, G. P., Milton, J., Brown, C. G., Hall, K. P., Evers, D. J., Barnes, C. L., Bignell, H. R., Boutell, J. M., Bryant, J., Carter, R. J., Keira Cheetham, R., Cox, A. J., Ellis, D. J., Flatbush, M. R., Gormley, N. A., Humphray, S. J., … Smith, A. J. (2008). Accurate whole human genome sequencing using reversible terminator chemistry. *Nature*, *456*(7218), 53–59. https://doi.org/10.1038/nature07517

Bokulich, N. A., Kaehler, B. D., Rideout, J. R., Dillon, M., Bolyen, E., Knight, R., Huttley, G. A., & Gregory Caporaso, J. (2018). Optimizing taxonomic classification of marker-gene amplicon sequences with QIIME 2's q2-feature-classifier plugin. *Microbiome*, *6*(1), 90. https://doi.org/10.1186/s40168-018-0470-z

Bolyen, E., Rideout, J. R., Dillon, M. R., Bokulich, N. A., Abnet, C. C., Al-Ghalith, G. A., Alexander, H., Alm, E. J., Arumugam, M., Asnicar, F., Bai, Y., Bisanz, J. E., Bittinger, K., Brejnrod, A., Brislawn, C. J., Brown, C. T., Callahan, B. J., Caraballo-Rodríguez, A. M., Chase, J., … Caporaso, J. G. (2019). Reproducible, interactive, scalable and extensible microbiome data science using QIIME 2. *Nature Biotechnology*, *37*(8), 852–857. https://doi.org/10.1038/s41587-019-0209-9

Brefort, T., Doehlemann, G., Mendoza-Mendoza, A., Reissmann, S., Djamei, A., & Kahmann, R. (2009). Ustilago maydis as a Pathogen. *Annual Review of Phytopathology*, *47*(1), 423–445. https://doi.org/10.1146/annurev-phyto-080508-081923

Brooks, M., E., Kristensen, K., Benthem, K., J. ,van, Magnusson, A., Berg, C., W., Nielsen, A., Skaug, H., J., Mächler, M., & Bolker, B., M. (2017). glmmTMB Balances Speed and Flexibility Among Packages for Zero-inflated Generalized Linear Mixed Modeling. *The R Journal*, *9*(2), 378. https://doi.org/10.32614/RJ-2017-066

Callahan, B. J., McMurdie, P. J., Rosen, M. J., Han, A. W., Johnson, A. J. A., & Holmes, S. P. (2016). DADA2: High-resolution sample inference from Illumina amplicon data. *Nature Methods*, *13*(7), 581–583. https://doi.org/10.1038/nmeth.3869

Cao, X., Duan, X., Zhou, Y., & Luo, Y. (2012). Dynamics in concentrations of Blumeria graminis f. Sp tritici conidia and its relationship to local weather conditions and disease index in wheat. *European Journal of Plant Pathology*, *132*(4), 525–535. https://doi.org/10.1007/s10658-011-9898-8

Carisse, O., Fall, M. L., & Vincent, C. (2017). Using a biovigilance approach for pest and disease management in Quebec vineyards. *Canadian Journal of Plant Pathology*, *39*(4), 393–404. https://doi.org/10.1080/07060661.2017.1366368

Carris, L. M., Castlebury, L. A., & Goates, B. J. (2006). Nonsystemic Bunt Fungi— *Tilletia indica* and *T. horrida*: A Review of History, Systematics, and Biology. *Annual Review of Phytopathology*, *44*(1), 113–133. https://doi.org/10.1146/annurev.phyto.44.070505.143402

Chen, W., Wellings, C., Chen, X., Kang, Z., & Liu, T. (2014). Wheat stripe (yellow) rust caused by *P uccinia striiformis* f. Sp. *Tritici*. *Molecular Plant Pathology*, *15*(5), 433–446. https://doi.org/10.1111/mpp.12116

Chen, W., Hambleton, S., Seifert, K. A., Carisse, O., Diarra, M. S., Peters, R. D., Lowe, C., Chapados, J. T., & Lévesque, C. A. (2018). Assessing Performance of Spore Samplers in Monitoring Aeromycobiota and Fungal Plant Pathogen Diversity in Canada. *Applied and Environmental Microbiology*, *84*(9), e02601-17. https://doi.org/10.1128/AEM.02601-17

Chen, W., Radford, D., & Hambleton, S. (2022). Towards Improved Detection and Identification of Rust Fungal Pathogens in Environmental Samples Using a Metabarcoding Approach. *Phytopathology*, *112*(3), 535–548. https://doi.org/10.1094/PHYTO-01-21-0020-R

Chen, W., Newlands, N., Hambleton, S., Laroche, A., Davoodi, S. M., & Bakkeren, G. (2024). Optimizing an integrated biovigilance toolbox to study the spatial distribution and dynamic changes of airborne mycobiota, with a focus on cereal rust fungi in western Canada. *Molecular Ecology Resources*, *24*(6), e13983. https://doi.org/10.1111/1755-0998.13983

Cheng, C., Xu, S., Liu, Z., Zhang, H., Yang, Y., Zhang, Y., Ge, E., Xu, J., Zhu, Q., Li, X., Yu, B., Liu, M., & Guo, Y. (2026). Microbial community differences between healthy and Ustilago-infected oats. *Genomics*, *118*(2), 111202. https://doi.org/10.1016/j.ygeno.2026.111202

Chuan, J., Zhou, A., Hale, L. R., He, M., & Li, X. (2021). Atria: An ultra-fast and accurate trimmer for adapter and quality trimming. *Gigabyte*, *2021*, 1–18. https://doi.org/10.46471/gigabyte.31

Cobo-Díaz, J. F., Baroncelli, R., Le Floch, G., & Picot, A. (2019). A novel metabarcoding approach to investigate Fusarium species composition in soil and plant samples. *FEMS Microbiology Ecology*, *95*(7), fiz084. https://doi.org/10.1093/femsec/fiz084

Comeau, A. M., Douglas, G. M., & Langille, M. G. I. (2017). Microbiome Helper: A Custom and Streamlined Workflow for Microbiome Research. *mSystems*, *2*(1), e00127-16. https://doi.org/10.1128/mSystems.00127-16

Comeau, A., & Kwawukume, A. (2022). *Preparing multiplexed 16S/18S/ITS amplicons for the Illumina MiSeq v1*. https://doi.org/10.17504/protocols.io.4r3l277k3g1y/v1

Cowger, C., Parks, R., & Kosman, E. (2016). Structure and Migration in U.S. *Blumeria graminis* f. Sp. *Tritici* Populations. *Phytopathology®*, *106*(3), 295–304. https://doi.org/10.1094/PHYTO-03-15-0066-R

Cowger, C., Ward, B., Brown-Guedira, G., & Brown, J. K. M. (2020). Role of Effector-Sensitivity Gene Interactions and Durability of Quantitative Resistance to Septoria Nodorum Blotch in Eastern U.S. Wheat. *Frontiers in Plant Science*, *11*, 155. https://doi.org/10.3389/fpls.2020.00155

Dawson, N., Fischer, J., Kuhn, M., Pasotti, A., Rouzaud, D., mhugent, Bruy, A., Sutton, T., Dobias, M., Pellerin, M., Rouault, E., Olaya, V., Blottiere, P., Macho, W., Cabieces, J., Blazek, R., Bartoletti, L., Sherman, G., Sant-anna, H., … Jurgiel, B. (2026). *qgis/QGIS: 3.44.13* (Version final-3_44_13) [Computer software]. Zenodo. https://doi.org/10.5281/ZENODO.6139224

Dietzel, K., Valle, D., Fierer, N., U'Ren, J. M., & Barberán, A. (2019). Geographical Distribution of Fungal Plant Pathogens in Dust Across the United States. *Frontiers in Ecology and Evolution*, *7*, 304. https://doi.org/10.3389/fevo.2019.00304

Downie, R. C., Lin, M., Corsi, B., Ficke, A., Lillemo, M., Oliver, R. P., Phan, H. T. T., Tan, K.-C., & Cockram, J. (2021). Septoria Nodorum Blotch of Wheat: Disease Management and Resistance Breeding in the Face of Shifting Disease Dynamics and a Changing Environment. *Phytopathology®*, *111*(6), 906–920. https://doi.org/10.1094/PHYTO-07-20-0280-RVW

Eddy, S. R. (1995). Multiple alignment using hidden Markov models. *Ismb*, *3*, 114–120.

Edgar, R. C. (2010). Search and clustering orders of magnitude faster than BLAST. *Bioinformatics*, *26*(19), 2460–2461. https://doi.org/10.1093/bioinformatics/btq461

Elad, Y., & Pertot, I. (2014). Climate Change Impacts on Plant Pathogens and Plant Diseases. *Journal of Crop Improvement*, *28*(1), 99–139. https://doi.org/10.1080/15427528.2014.865412

Elmhirst, J. (2023). Canadian Plant Disease Survey 2023 Volume 103: Disease Highlights 2022. *Canadian Journal of Plant Pathology*, *45*(sup1), 1–171. https://doi.org/10.1080/07060661.2023.2222486

Ferguson, R. M. W., Garcia-Alcega, S., Coulon, F., Dumbrell, A. J., Whitby, C., & Colbeck, I. (2019). Bioaerosol biomonitoring: Sampling optimization for molecular microbial ecology. *Molecular Ecology Resources*, *19*(3), 672–690. https://doi.org/10.1111/1755-0998.13002

Fernandez, M. R., Stevenson, C. F., Hodge, K., Dokken-Bouchard, F., Pearse, P. G., Waelchli, F., Brown, A., & Peluola, C. (2016). Assessing Effects of Climatic Change, Region and Agronomic Practices on Leaf Spotting of Bread and Durum Wheat in the Western Canadian Prairies, from 2001 to 2012. *Agronomy Journal*, *108*(3), 1180–1195. https://doi.org/10.2134/agronj2015.0451

Ferrigo, D., Raiola, A., & Causin, R. (2016). Fusarium Toxins in Cereals: Occurrence, Legislation, Factors Promoting the Appearance and Their Management. *Molecules*, *21*(5), 627. https://doi.org/10.3390/molecules21050627

Francisco, C. S., Ma, X., Zwyssig, M. M., McDonald, B. A., & Palma-Guerrero, J. (2019). Morphological changes in response to environmental stresses in the fungal plant pathogen Zymoseptoria tritici. *Scientific Reports*, *9*(1), 9642. https://doi.org/10.1038/s41598-019-45994-3

Gahagan, A. C., Shi, Y., Radford, D., Morrison, M. J., Gregorich, E., Aris-Brosou, S., & Chen, W. (2023). Long-Term Tillage and Crop Rotation Regimes Reshape Soil-Borne Oomycete Communities in Soybean, Corn, and Wheat Production Systems. *Plants*, *12*(12), 2338. https://doi.org/10.3390/plants12122338

Gaudet, D. A., Wang, Y., Penniket, C., Lu, Z. X., Bakkeren, G., & Laroche, A. (2010). Morphological and Molecular Analyses of Host and Nonhost Interactions Involving Barley and Wheat and the Covered Smut Pathogen *Ustilago hordei*. *Molecular Plant-Microbe Interactions®*, *23*(12), 1619–1634. https://doi.org/10.1094/MPMI-11-09-0271

Gautam, H. R., Bhardwaj, M. L., & Kumar, R. (2013). Climate change and its impact on plant diseases. *Current Science*, *105*(12), 1685–1691.

Golan, J. J., & Pringle, A. (2017). Long-Distance Dispersal of Fungi. *Microbiology Spectrum*, *5*(4), 5.4.03. https://doi.org/10.1128/microbiolspec.FUNK-0047-2016

Goswami, R. S., & Kistler, H. C. (2004). Heading for disaster: *Fusarium graminearum* on cereal crops. *Molecular Plant Pathology*, *5*(6), 515–525. https://doi.org/10.1111/j.1364-3703.2004.00252.x

Grinn-Gofroń, A., & Bosiacka, B. (2015). Effects of meteorological factors on the composition of selected fungal spores in the air. *Aerobiologia*, *31*(1), 63–72. https://doi.org/10.1007/s10453-014-9347-1

Hafez, M., Gourlie, R., Despins, T., Turkington, T. K., Friesen, T. L., & Aboukhaddour, R. (2020). *Parastagonospora nodorum* and Related Species in Western Canada: Genetic Variability and Effector Genes. *Phytopathology*®, *110*(12), 1946–1958. https://doi.org/10.1094/PHYTO-05-20-0207-R

Harris, L. J., Balcerzak, M., Johnston, A., Schneiderman, D., & Ouellet, T. (2016). Host-preferential Fusarium graminearum gene expression during infection of wheat, barley, and maize. *Fungal Biology*, *120*(1), 111–123. https://doi.org/10.1016/j.funbio.2015.10.010

Hellin, P., Duvivier, M., Dedeurwaerder, G., Bataille, C., De Proft, M., & Legrève, A. (2018). Evaluation of the temporal distribution of Fusarium graminearum airborne inoculum above the wheat canopy and its relationship with Fusarium head blight and DON concentration. *European Journal of Plant Pathology*, *151*(4), 1049–1064. https://doi.org/10.1007/s10658-018-1442-7

Hibbett, D., Abarenkov, K., Kõljalg, U., Öpik, M., Chai, B., Cole, J., Wang, Q., Crous, P., Robert, V., Helgason, T., Herr, J. R., Kirk, P., Lueschow, S., O'Donnell, K., Nilsson, R. H., Oono, R., Schoch, C., Smyth, C., Walker, D. M., … Geiser, D. M. (2016). Sequence-based classification and identification of Fungi. *Mycologia*, *108*(6), 1049–1068. https://doi.org/10.3852/16-130

Hoffmann, A., Posirca, A.-R., Lewin, S., Verch, G., Büttner, C., & Müller, M. E. H. (2023). Environmental Filtering Drives Fungal Phyllosphere Community in Regional Agricultural Landscapes. *Plants*, *12*(3), 507. https://doi.org/10.3390/plants12030507

Inuma, T., Khodaparast, S. A., & Takamatsu, S. (2007). Multilocus phylogenetic analyses within Blumeria graminis, a powdery mildew fungus of cereals. *Molecular Phylogenetics and Evolution*, *44*(2), 741–751. https://doi.org/10.1016/j.ympev.2007.01.007

Kahmann, R., & Kämper, J. (2004). *Ustilago maydis*: How its biology relates to pathogenic development. *New Phytologist*, *164*(1), 31–42. https://doi.org/10.1111/j.1469-8137.2004.01156.x

Karlsson, E., Johansson, A.-M., Ahlinder, J., Lundkvist, M. J., Singh, N. J., Brodin, T., Forsman, M., & Stenberg, P. (2020). Airborne microbial biodiversity and seasonality in Northern and Southern Sweden. *PeerJ*, *8*, e8424. https://doi.org/10.7717/peerj.8424

Karlsson, I., Edel-Hermann, V., Gautheron, N., Durling, M. B., Kolseth, A.-K., Steinberg, C., Persson, P., & Friberg, H. (2016). Genus-Specific Primers for Study of Fusarium Communities in Field Samples. *Applied and Environmental Microbiology*, *82*(2), 491–501. https://doi.org/10.1128/AEM.02748-15

Karlsson, I., Persson, P., & Friberg, H. (2021). Fusarium Head Blight From a Microbiome Perspective. *Frontiers in Microbiology*, *12*, 628373. https://doi.org/10.3389/fmicb.2021.628373

Katoh, K., & Standley, D. M. (2013). MAFFT Multiple Sequence Alignment Software Version 7: Improvements in Performance and Usability. *Molecular Biology and Evolution*, *30*(4), 772–780. https://doi.org/10.1093/molbev/mst010

Kutcher, H. R., Turkington, T. K., McLaren, D. L., Irvine, R. B., & Brar, G. S. (2018). Fungicide and Cultivar Management of Leaf Spot Diseases of Winter Wheat in Western Canada. *Plant Disease*, *102*(9), 1828–1833. https://doi.org/10.1094/PDIS-12-17-1920-RE

Lenth, R. V., & Piaskowski, J. (2017). *emmeans: Estimated Marginal Means, aka Least-Squares Means* (p. 2.0.4) [Dataset]. https://doi.org/10.32614/CRAN.package.emmeans

Letunic, I., & Bork, P. (2024). Interactive Tree of Life (iTOL) v6: Recent updates to the phylogenetic tree display and annotation tool. *Nucleic Acids Research*, *52*(W1), W78–W82. https://doi.org/10.1093/nar/gkae268

Liaw, A., & Wiener, M. (2002). Classification and regression by randomForest. *R news*, *2*(3), 18-22.

Loo, J. A. (2009). Ecological impacts of non-indigenous invasive fungi as forest pathogens. *Biological Invasions*, *11*(1), 81–96. https://doi.org/10.1007/s10530-008-9321-3

Lorrain, C., Gonçalves Dos Santos, K. C., Germain, H., Hecker, A., & Duplessis, S. (2019). Advances in understanding obligate biotrophy in rust fungi. *New Phytologist*, *222*(3), 1190–1206. https://doi.org/10.1111/nph.15641

Lücking, R., Aime, M. C., Robbertse, B., Miller, A. N., Ariyawansa, H. A., Aoki, T., Cardinali, G., Crous, P. W., Druzhinina, I. S., Geiser, D. M., Hawksworth, D. L., Hyde, K. D., Irinyi, L., Jeewon, R., Johnston, P. R., Kirk, P. M., Malosso, E., May, T. W., Meyer, W., … Schoch, C. L. (2020). Unambiguous identification of fungi: Where do we stand and how accurate and precise is fungal DNA barcoding? *IMA Fungus*, *11*(1), 14. https://doi.org/10.1186/s43008-020-00033-z

Lyon, B., & Broders, K. (2017). Impact of climate change and race evolution on the epidemiology and ecology of stripe rust in central and eastern USA and Canada. *Canadian Journal of Plant Pathology*, *39*(4), 385–392. https://doi.org/10.1080/07060661.2017.1368713

MacKenzie, M., & Argyropoulos, C. (2023). An Introduction to Nanopore Sequencing: Past, Present, and Future Considerations. *Micromachines*, *14*(2), 459. https://doi.org/10.3390/mi14020459

Magarey, R. D., Colunga-Garcia, M., & Fieselmann, D. A. (2009). Plant Biosecurity in the United states: Roles, Responsibilities, and Information Needs. *BioScience*, *59*(10), 875–884. https://doi.org/10.1525/bio.2009.59.10.9

Mahas, J. W., Wilson, A. E., Steury, T. D., & Jacobson, A. L. (2026). Association of plant pathogen vectors and vector-borne plant pathogens with landscape composition: A meta-analysis. *Environmental Entomology*, *55*(1), nvaf120. https://doi.org/10.1093/ee/nvaf120

Manstretta, V., & Rossi, V. (2015). Effects of Weather Variables on Ascospore Discharge from Fusarium graminearum Perithecia. *PLOS ONE*, *10*(9), e0138860. https://doi.org/10.1371/journal.pone.0138860

Mapuranga, J., Zhang, N., Zhang, L., Chang, J., & Yang, W. (2022). Infection Strategies and Pathogenicity of Biotrophic Plant Fungal Pathogens. *Frontiers in Microbiology*, *13*, 799396. https://doi.org/10.3389/fmicb.2022.799396

Mapuranga, J., Chang, J., & Yang, W. (2022b). Combating powdery mildew: Advances in molecular interactions between Blumeria graminis f. sp. tritici and wheat. *Frontiers in Plant Science*, *13*, 1102908. https://doi.org/10.3389/fpls.2022.1102908

Martin, M. (2011). Cutadapt removes adapter sequences from high-throughput sequencing reads. *EMBnet.Journal*, *17*(1), 10. https://doi.org/10.14806/ej.17.1.200

Marzec-Schmidt, K., Börjesson, T., Suproniene, S., Jędryczka, M., Janavičienė, S., Góral, T., Karlsson, I., Kochiieru, Y., Ochodzki, P., Mankevičienė, A., & Piikki, K. (2021). Modelling the Effects of Weather Conditions on Cereal Grain Contamination with Deoxynivalenol in the Baltic Sea Region. *Toxins*, *13*(11), 737. https://doi.org/10.3390/toxins13110737

Mathre, D. E. (1997). *Compendium of barley diseases* (Vol. 90). D. E. Mathre (Ed.). St. Paul, MN: APS press.

McCallum, B. D., Geddes, C. M., Chatterton, S., Peng, G., Carisse, O., Turkington, T. K., Olfert, O., Leeson, J., Sharpe, S., Stephens, E., Hervet, V., Aboukhaddour, R., & Vankosky, M. (2021). We stand on guard for thee: A brief history of pest surveillance on the Canadian Prairies. *Crop Protection*, *149*, 105748. https://doi.org/10.1016/j.cropro.2021.105748

McDonald, B. A., Suffert, F., Bernasconi, A., & Mikaberidze, A. (2022). How large and diverse are field populations of fungal plant pathogens? The case of *Zymoseptoria tritici*. *Evolutionary Applications*, *15*(9), 1360–1373. https://doi.org/10.1111/eva.13434

Meyer, M., Burgin, L., Hort, M. C., Hodson, D. P., & Gilligan, C. A. (2017). Large-Scale Atmospheric Dispersal Simulations Identify Likely Airborne Incursion Routes of Wheat Stem Rust Into Ethiopia. *Phytopathology®*, *107*(10), 1175–1186. https://doi.org/10.1094/PHYTO-01-17-0035-FI

Miedaner, T., & Geiger, H. (2015). Biology, Genetics, and Management of Ergot (Claviceps spp.) in Rye, Sorghum, and Pearl Millet. *Toxins*, *7*(3), 659–678. https://doi.org/10.3390/toxins7030659

Mohite, B. V., Koli, S. H., Salunkhe, J. D., & Patil, S. V. (2025). Ustilago. In N. Amaresan & K. Kumar (Eds.), *Compendium of Phytopathogenic Microbes in Agro-Ecology* (pp. 909–925). Springer Nature Switzerland. https://doi.org/10.1007/978-3-031-81770-0_38

Moore, D. (2020). *21st Century Guidebook to Fungi—SECOND EDITION - Reviews and Contents*.

Moore, S. M., & Borer, E. T. (2012). The influence of host diversity and composition on epidemiological patterns at multiple spatial scales. *Ecology*, *93*(5), 1095–1105. https://doi.org/10.1890/11-0086.1

Nguyen, N. H., Song, Z., Bates, S. T., Branco, S., Tedersoo, L., Menke, J., Schilling, J. S., & Kennedy, P. G. (2016). FUNGuild: An open annotation tool for parsing fungal community datasets by ecological guild. *Fungal Ecology*, *20*, 241–248. https://doi.org/10.1016/j.funeco.2015.06.006

Nilsson, R. H., Larsson, K.-H., Taylor, A. F. S., Bengtsson-Palme, J., Jeppesen, T. S., Schigel, D., Kennedy, P., Picard, K., Glöckner, F. O., Tedersoo, L., Saar, I., Kõljalg, U., & Abarenkov, K. (2019). The UNITE database for molecular identification of fungi: Handling dark taxa and parallel taxonomic classifications. *Nucleic Acids Research*, *47*(D1), D259–D264. https://doi.org/10.1093/nar/gky1022

Paradis, E., & Schliep, K. (2019). ape 5.0: An environment for modern phylogenetics and evolutionary analyses in R. *Bioinformatics*, *35*(3), 526–528. https://doi.org/10.1093/bioinformatics/bty633

Pilo, P., Lawless, C., Tiley, A. M. M., Karki, S. J., Burke, J. I., & Feechan, A. (2022). Comparison of microscopic and metagenomic approaches to identify cereal pathogens and track fungal spore release in the field. *Frontiers in Plant Science*, *13*, 1039090. https://doi.org/10.3389/fpls.2022.1039090

Prank, M., Kenaley, S. C., Bergstrom, G. C., Acevedo, M., & Mahowald, N. M. (2019). Climate change impacts the spread potential of wheat stem rust, a significant crop disease. *Environmental Research Letters*, *14*(12), 124053. https://doi.org/10.1088/1748-9326/ab57de

Reich, J., Chatterton, S., & Johnson, D. (2017). Temporal Dynamics of *Botrytis cinerea* and *Sclerotinia sclerotiorum* in Seed Alfalfa Fields of Southern Alberta, Canada. *Plant Disease*, *101*(2), 331–343. https://doi.org/10.1094/PDIS-04-16-0492-RE

Reich, J., Chen, W., Radford, D., Turkington, K., Yevtushenko, D., Hamelin, R., & Chatterton, S. (2023). Combining Air Sampling and DNA Metabarcoding to Monitor Plant Pathogens. *PhytoFrontiers™*, *3*(3), 639–653. https://doi.org/10.1094/PHYTOFR-10-22-0108-R

Rogers, S. L., Atkins, S. D., & West, J. S. (2009). Detection and quantification of airborne inoculum of *Sclerotinia sclerotiorum* using quantitative PCR. *Plant Pathology*, *58*(2), 324–331. https://doi.org/10.1111/j.1365-3059.2008.01945.x

Różewicz, M., Wyzińska, M., & Grabiński, J. (2021). The Most Important Fungal Diseases of Cereals—Problems and Possible Solutions. *Agronomy*, *11*(4), 714. https://doi.org/10.3390/agronomy11040714

Savary, S., Bregaglio, S., Willocquet, L., Gustafson, D., Mason D'Croz, D., Sparks, A., Castilla, N., Djurle, A., Allinne, C., Sharma, M., Rossi, V., Amorim, L., Bergamin, A., Yuen, J., Esker, P., McRoberts, N., Avelino, J., Duveiller, E., Koo, J., & Garrett, K. (2017). Crop health and its global impacts on the components of food security. *Food Security*, *9*(2), 311–327. https://doi.org/10.1007/s12571-017-0659-1

Sawyer, E. N., Kerr, W. A., & Hobbs, J. E. (2008). Consumer preferences and the international harmonization of organic standards. *Food Policy*, *33*(6), 607–615. https://doi.org/10.1016/j.foodpol.2008.04.006

Schoch, C. L., Seifert, K. A., Huhndorf, S., Robert, V., Spouge, J. L., Levesque, C. A., Chen, W., Fungal Barcoding Consortium, Fungal Barcoding Consortium Author List, Bolchacova, E., Voigt, K., Crous, P. W., Miller, A. N., Wingfield, M. J., Aime, M. C., An, K.-D., Bai, F.-Y., Barreto, R. W., Begerow, D., … Schindel, D. (2012). Nuclear ribosomal internal transcribed spacer (ITS) region as a universal DNA barcode marker for *Fungi*. *Proceedings*

of the National Academy of Sciences, *109*(16), 6241–6246. https://doi.org/10.1073/pnas.1117018109

Seethapathy, P. (2025). Tilletia. In Compendium of Phytopathogenic Microbes in Agro-Ecology: Vol. 1 Fungi (pp. 855-872). Springer.

Stakman, E. C., & Christensen, C. M. (1946). Aerobiology in relation to plant disease. *The Botanical Review*, *12*(4), 205–253. https://doi.org/10.1007/BF02861523

Stat Canada. (2024). Estimated areas, yield, production, average farm price and total farm value of principal field crops, in metric and imperial units.

Team, R. C. (2025). R: A Language and Environment for Statistical Computing. In https://www.R-project.org/

Van Der Heyden, H., Dutilleul, P., Charron, J.-B., Bilodeau, G. J., & Carisse, O. (2021). Monitoring airborne inoculum for improved plant disease management. A review. *Agronomy for Sustainable Development*, *41*(3), 40. https://doi.org/10.1007/s13593-021-00694-z

Wang, S., Gutell, R. R., & Miranker, D. P. (2007). Biclustering as a method for RNA local multiple sequence alignment. *Bioinformatics*, *23*(24), 3289–3296. https://doi.org/10.1093/bioinformatics/btm485

West, J. S., Canning, G. G. M., Perryman, S. A., & King, K. (2017). Novel Technologies for the detection of Fusarium head blight disease and airborne inoculum. *Tropical Plant Pathology*, *42*(3), 203–209. https://doi.org/10.1007/s40858-017-0138-4

Wong, T., Ly-Trong, N., Ren, H., Baños, H., Roger, A., Susko, E., Bielow, C., De Maio, N., Goldman, N., Hahn, M., Huttley, G., Lanfear, R., & Minh, B. Q. (2025). *IQ-TREE 3: Phylogenomic Inference Software using Complex Evolutionary Models*. Life Sciences. https://doi.org/10.32942/X2P62N

Wu, L., Hwang, S.-F., Strelkov, S. E., Fredua-Agyeman, R., Oh, S.-H., Bélanger, R. R., Wally, O., & Kim, Y.-M. (2024). Pathogenicity, Host Resistance, and Genetic Diversity of Fusarium Species under Controlled Conditions from Soybean in Canada. *Journal of Fungi*, *10*(5), 303. https://doi.org/10.3390/jof10050303

Zahariev, M., Chen, W., Visagie, C. M., & Lévesque, C. A. (2018). Cluster oligonucleotide signatures for rapid identification by sequencing. BMC Bioinformatics, 19(1), 395. https://doi.org/10.1186/s12859-018-2363-3

Zhan, G., Tian, Y., Wang, F., Chen, X., Guo, J., Jiao, M., Huang, L., & Kang, Z. (2014). A Novel Fungal Hyperparasite of Puccinia striiformis f. Sp. Tritici, the Causal Agent of Wheat Stripe Rust. *PLoS ONE*, *9*(11), e111484. https://doi.org/10.1371/journal.pone.0111484

Supplementary Figures and Tables

Supplementary figures

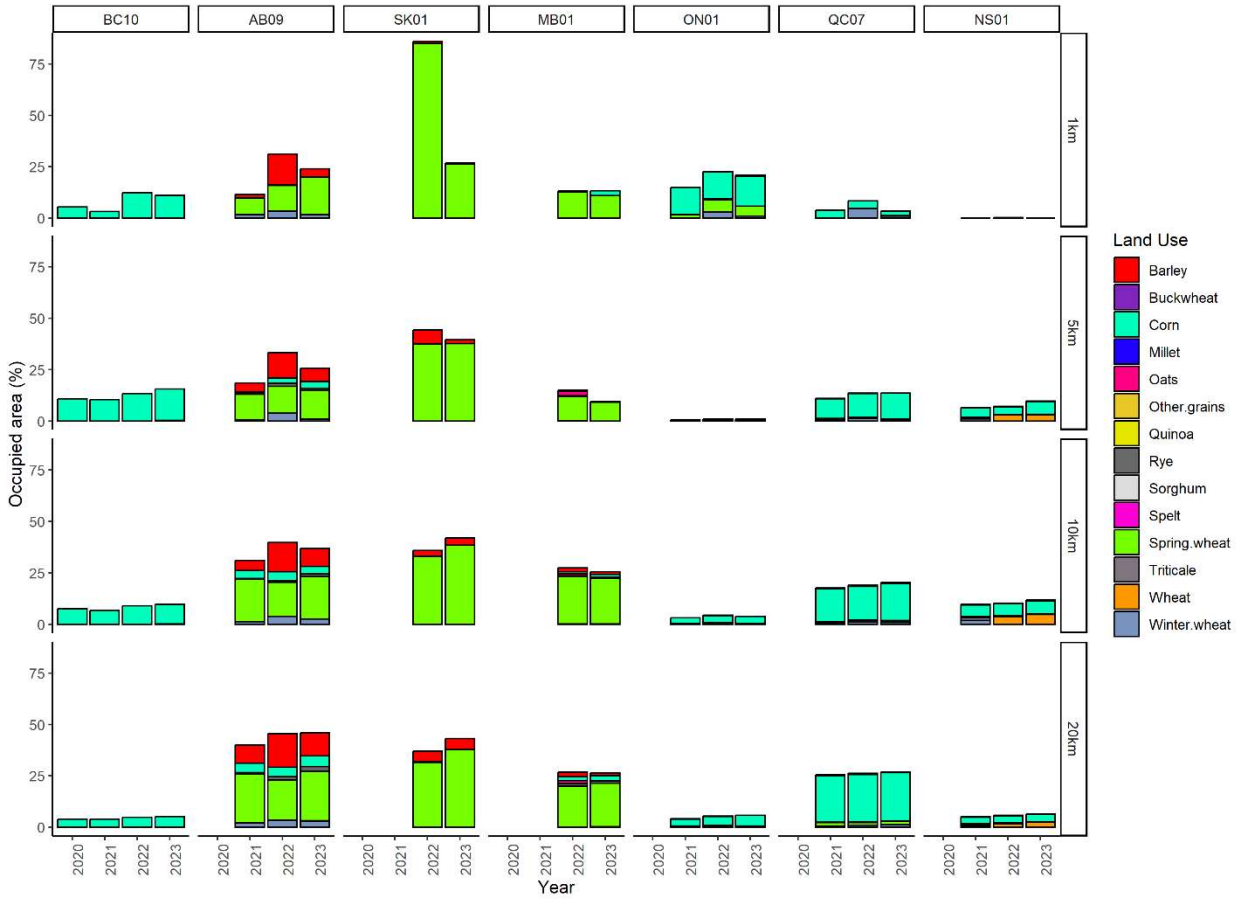

Figure S1. Land use proportions of cereals at each site in percentage of occupied area. Stacked bar plots show the percentage of cereal crop types within the given radius (in kilometers). BC, ON, QC, and NS have a strong focus on corn, while AB, SK, and MB are primarily wheat. AB also contains a lot of barley.

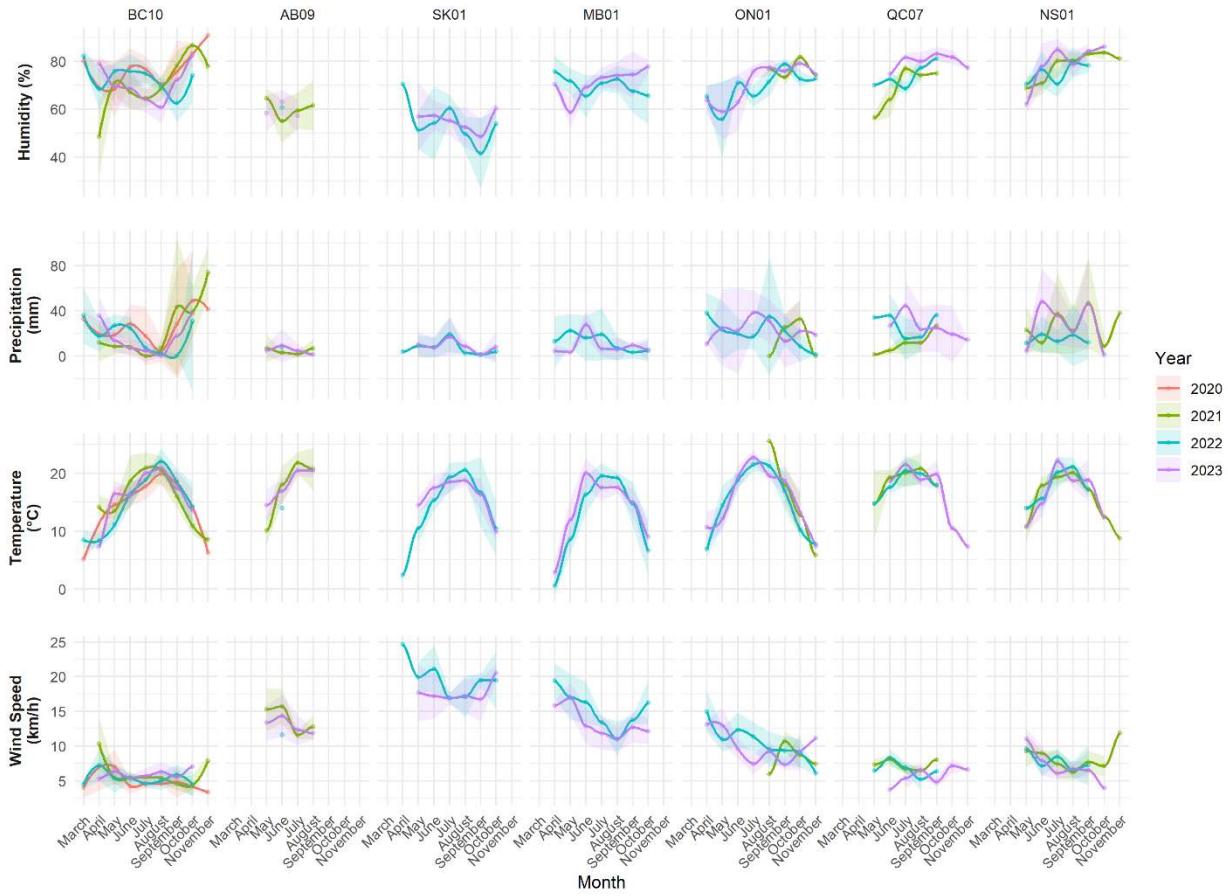

Figure S2. Temporal variation for weather conditions at each site. Error ribbon is in standard deviation.

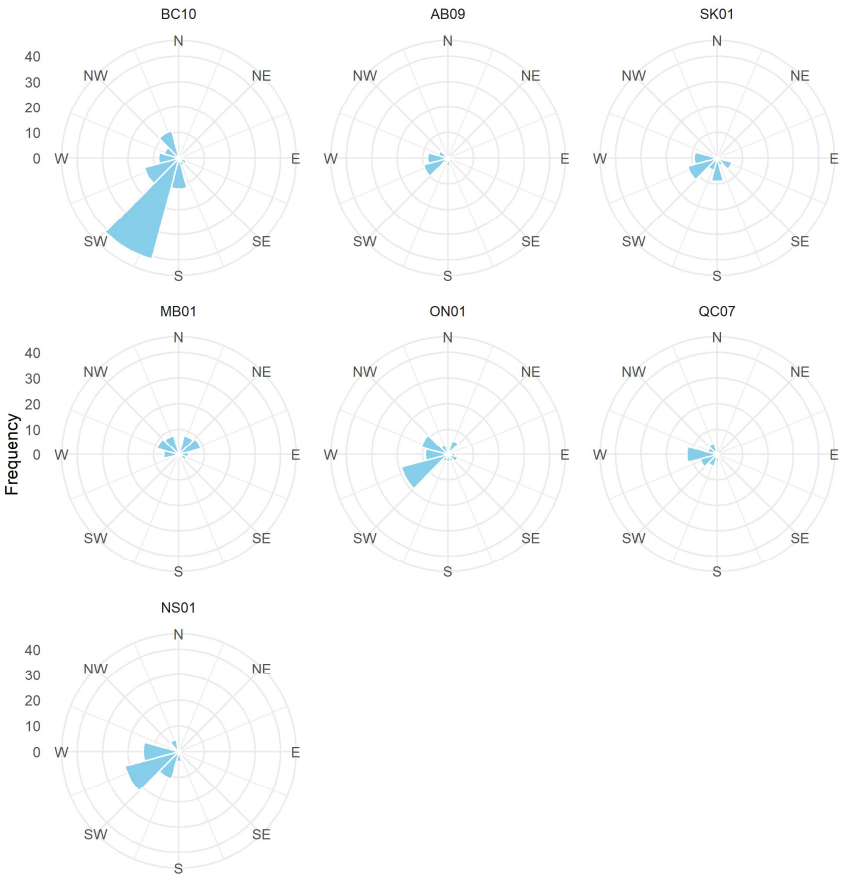

Figure S3. Wind direction by frequency at each site.

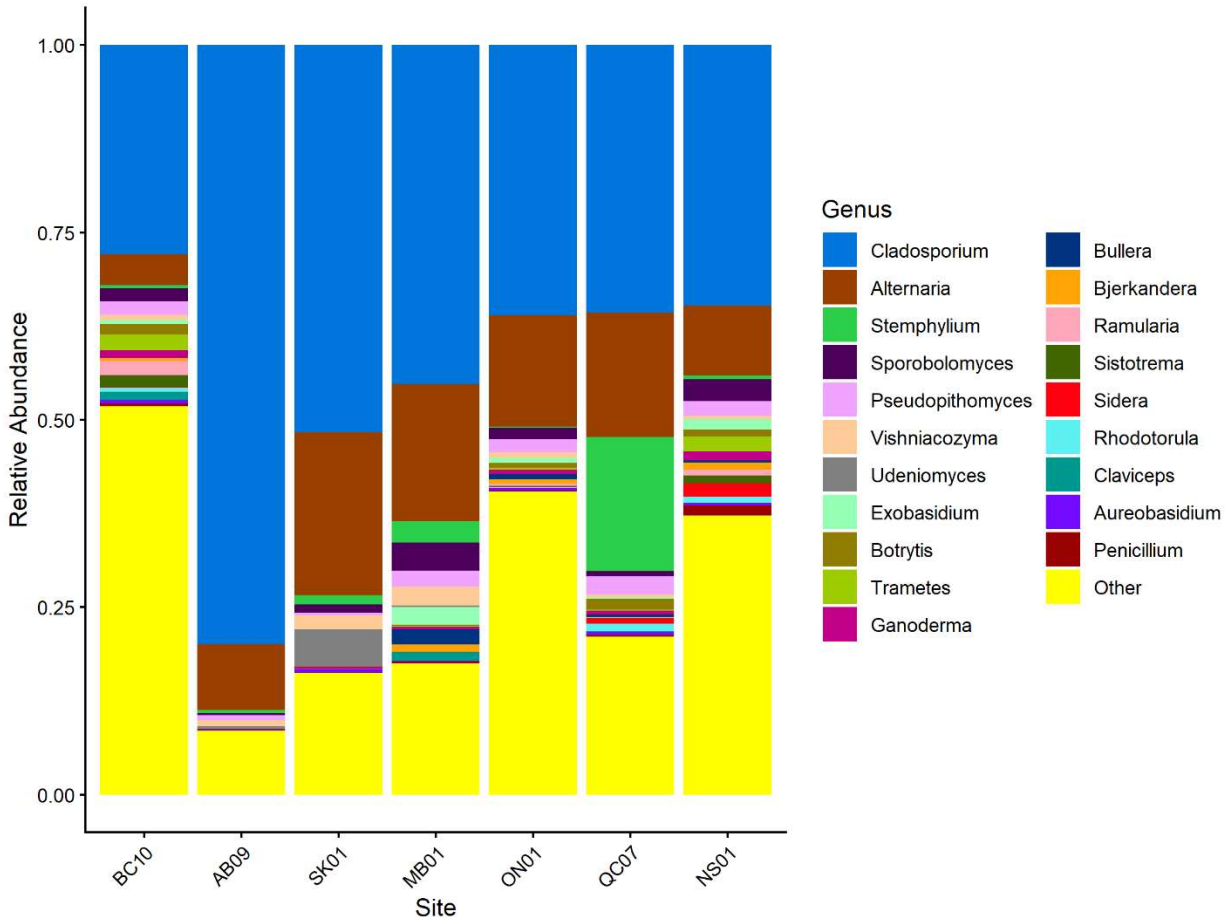

Figure S4. Stacked bar chart showing the relative abundance of the top 20 most abundant fungal genera across sampling sites and all years. Genera outside the top 20, including *Incertae sedis* taxa, are grouped as "Other". Relative abundances are averaged across samples within each site.

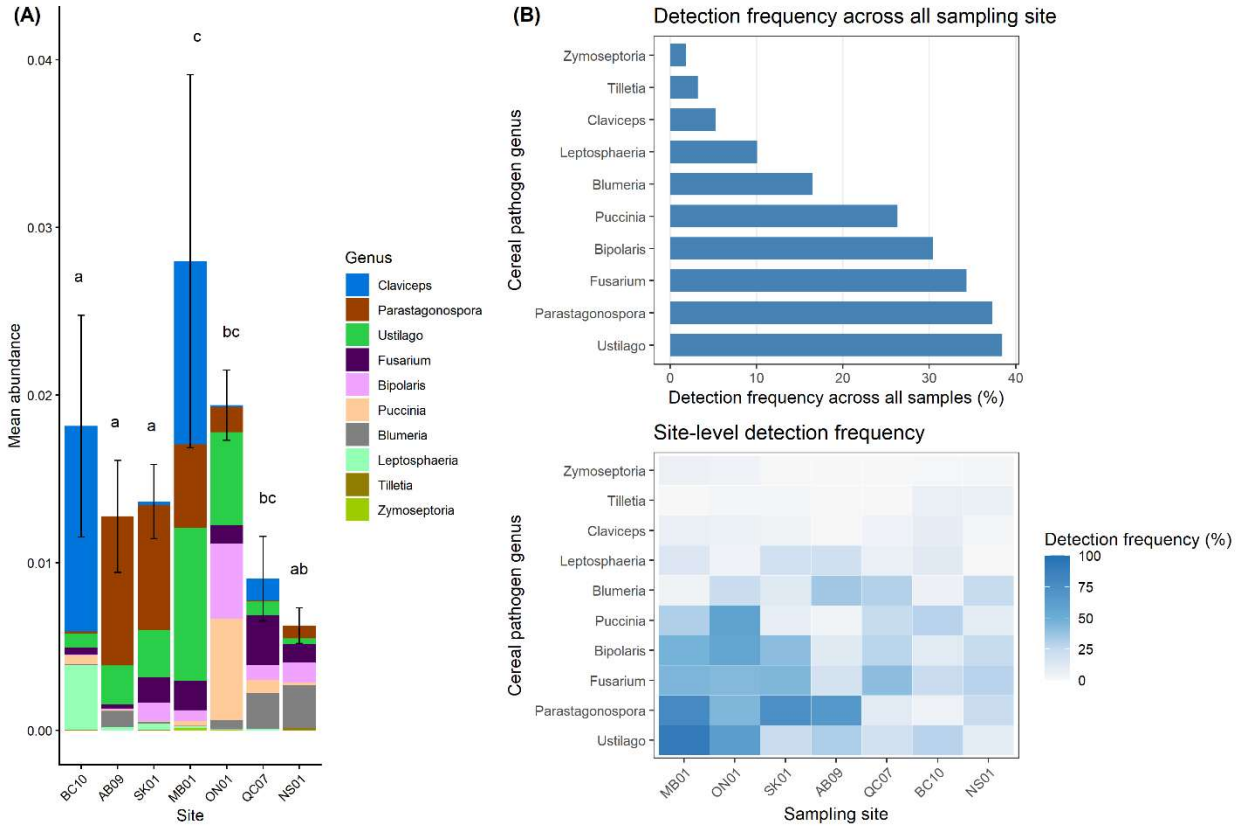

Figure S5. (A) Stacked bar chart showing the mean relative abundance of ten important cereal-associated fungal pathogen genera across sampling sites and all years. Each bar represents the site-level average genus composition (± standard error), with colors distinguishing genera. Error bars indicate the standard error of the total abundance at each site. Letters above bars denote groupings from multiple comparisons of total abundance (CLD test, $\alpha = 0.05$, Sidak adjustment); different letters indicate statistically significant differences. (B) Detection frequency of ten important cereal-associated genera across all sampling sites (top panel) and at each individual site (bottom panel).

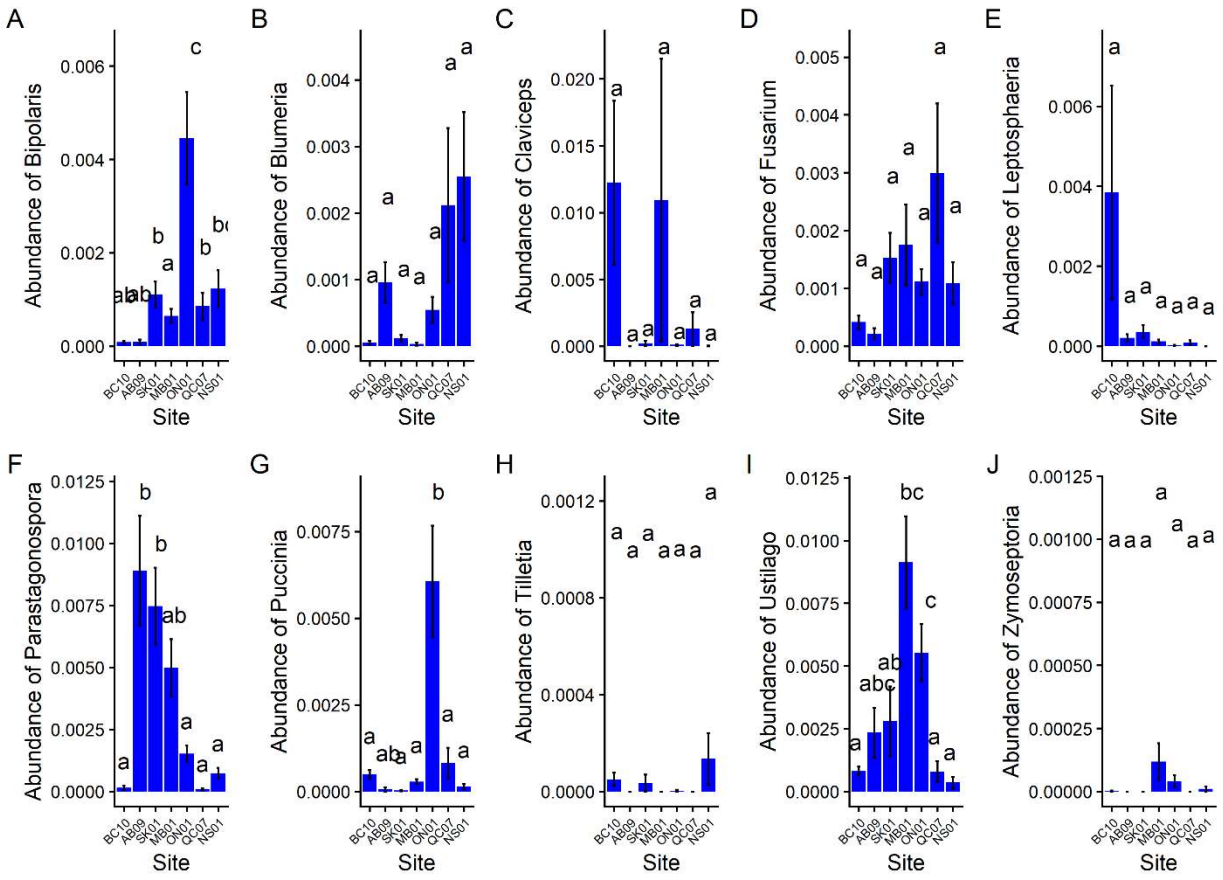

Figure S6. Relative abundance for each genus at each site. Error bars are in standard error. Letters denote compact letter display for significance; sites sharing a letter are not significantly different ($p > 0.05$).

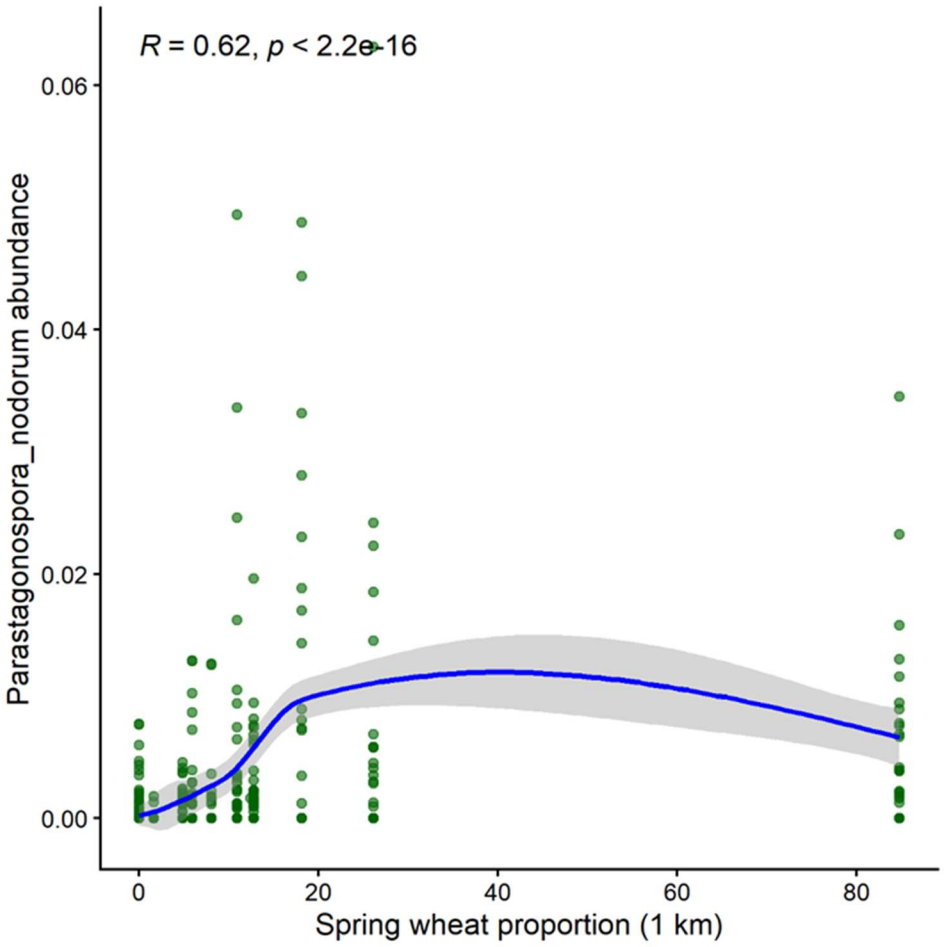

Figure S7. Correlation between *Parastagonospora nodorum* abundance and spring wheat proportion within a 1 km radius, assessed using Spearman's rank correlation.

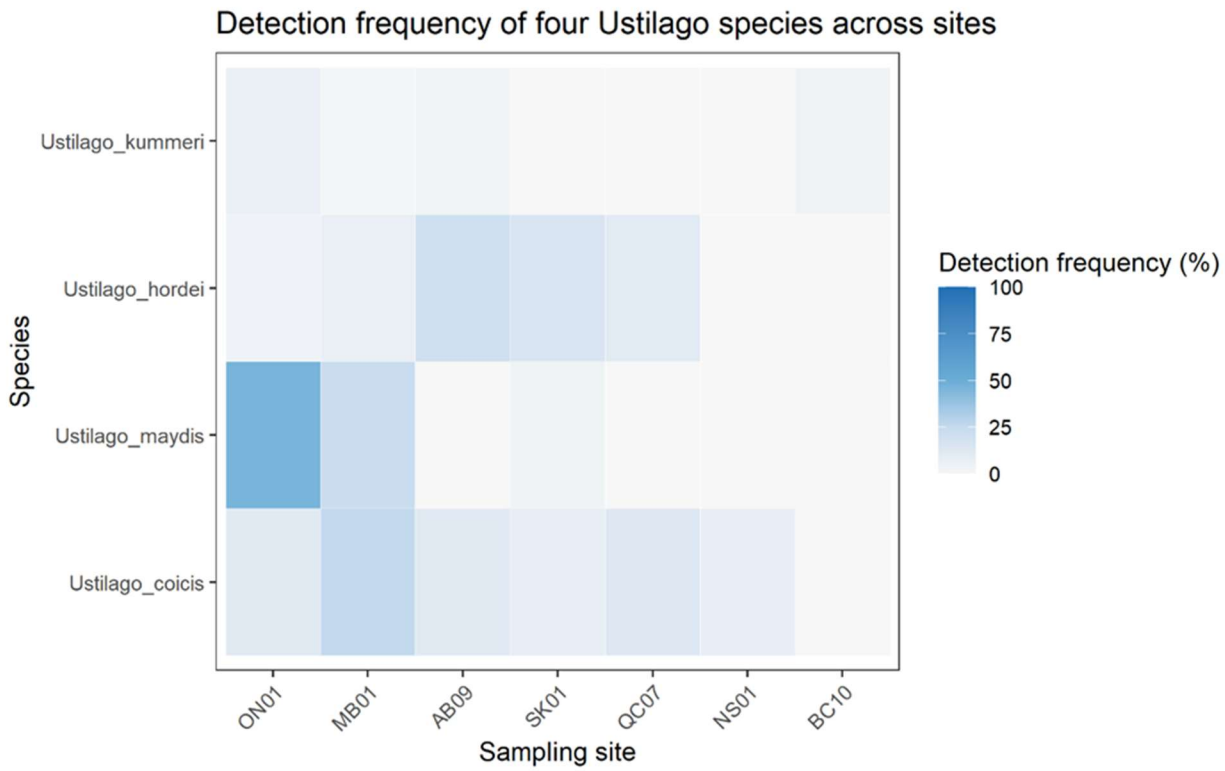

Figure S8. Detection frequency of four *Ustilago* species across sampling sites.

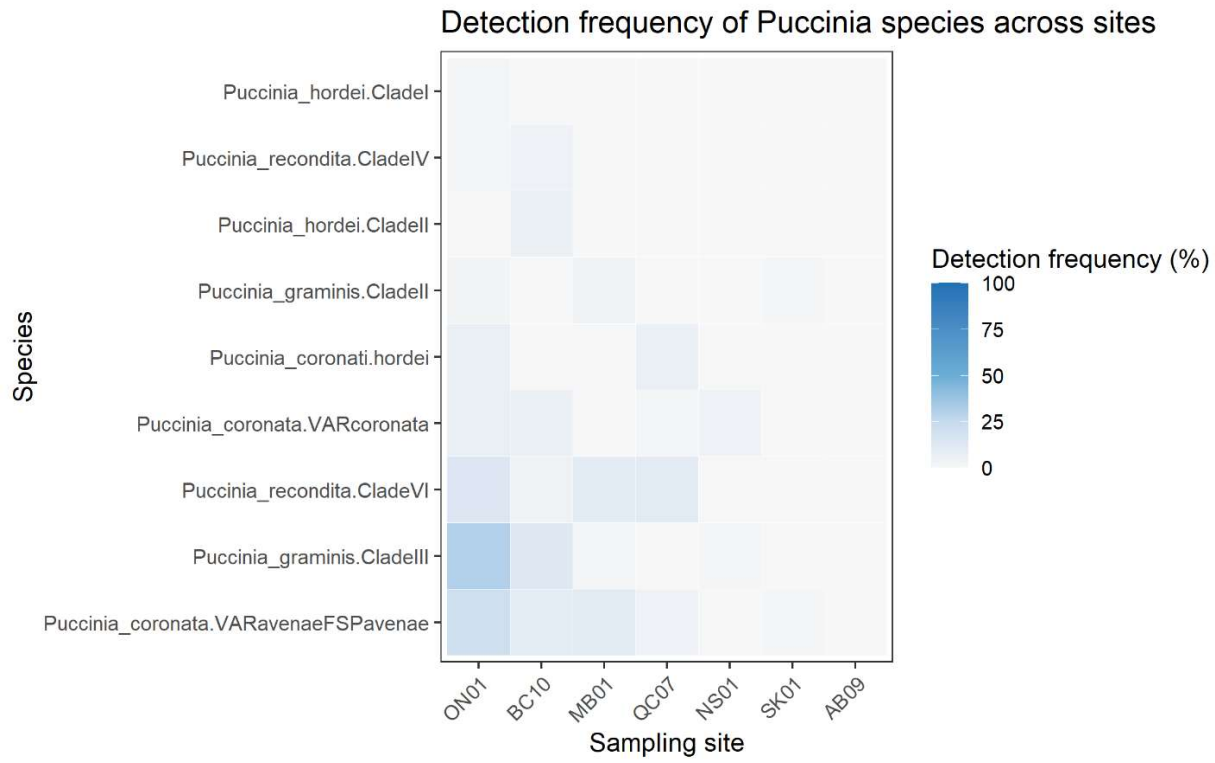

Figure S9. Detection frequency of *Puccinia* species across sites.

Supplementary tables

Table S1. Mean and standard deviation across all sites for the most abundant genera containing potential pathogens.

Genus	Mean relative abundance	Standard Deviation
Cladosporium	0.5531	0.2157
Alternaria	0.1935	0.1569
Stemphylium	0.0430	0.1288
Pseudopithomyces	0.0324	0.0572
Trametes	0.0133	0.0558
Botrytis	0.0124	0.0271
Bjerkandera	0.0117	0.0459
Exobasidium	0.0113	0.0345
Ramularia	0.0089	0.0366
Ganoderma	0.0087	0.0216
Peniophora	0.0086	0.0259
Ustilago	0.0085	0.0307
Puccinia	0.0077	0.0465
Periconia	0.0065	0.0177
Aureobasidium	0.0057	0.0172
Fusarium	0.0041	0.0144
Penicillium	0.0038	0.0420

Fomes	0.0038	0.0173
Rhodotorula	0.0031	0.0216
Taphrina	0.0031	0.0133
Other Genera	0.0567	0.0851

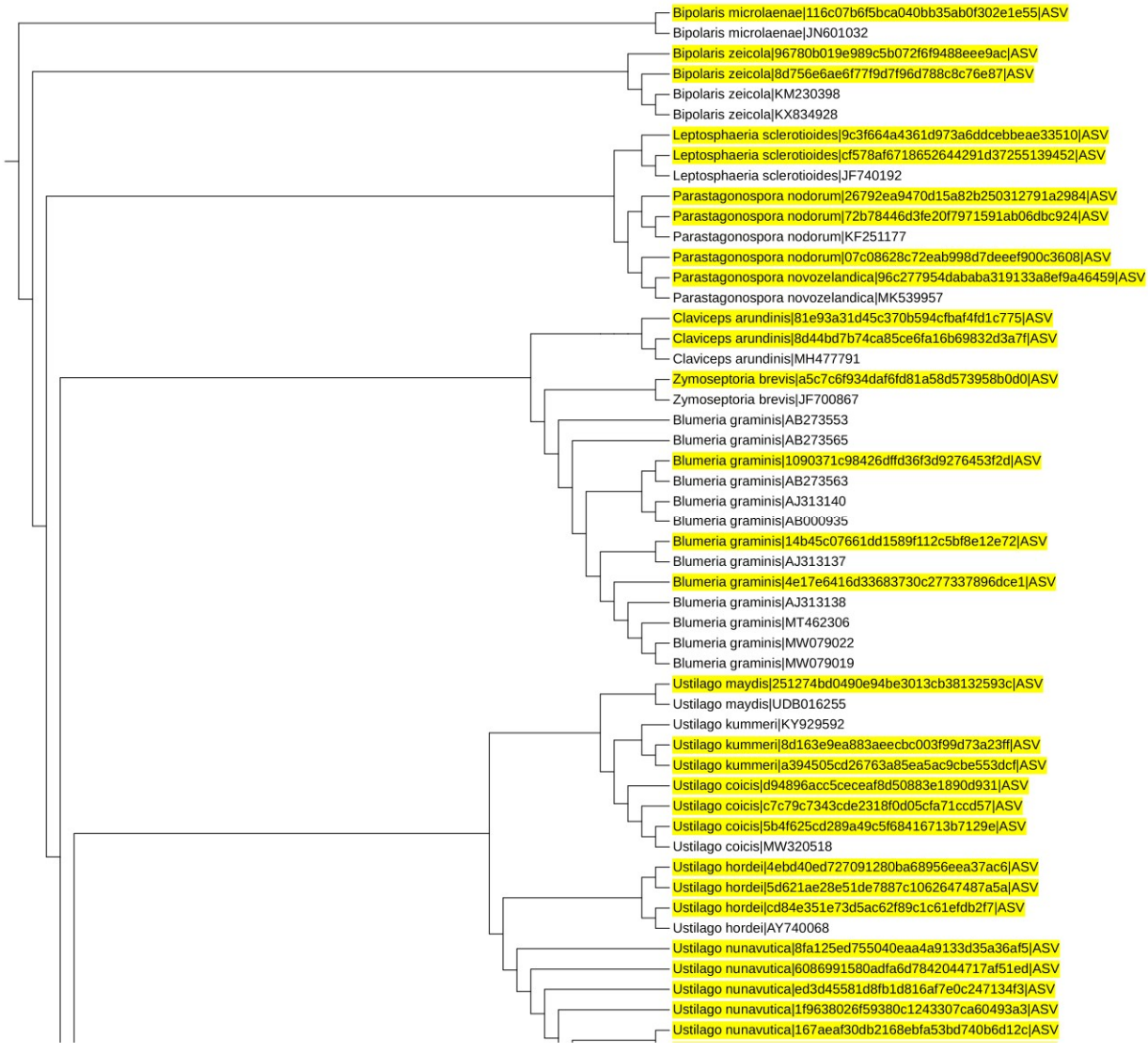
Bipolaris microlaenae|116c07b6f5bca040bb35ab0f302e1e55|ASV
Bipolaris microlaenae|JN601032
Bipolaris zeicola|96780b019e989c5b072f6f9488eee9ac|ASV
Bipolaris zeicola|8d756e6ae6f77f9d7f96d788c8c76e87|ASV
Bipolaris zeicola|KM230398
Bipolaris zeicola|KX834928
Leptosphaeria sclerotioides|9c3f664a4361d973a6ddcebbeae33510|ASV
Leptosphaeria sclerotioides|cf578af6718652644291d37255139452|ASV
Leptosphaeria sclerotioides|JF740192
Parastagonospora nodorum|26792ea9470d15a82b250312791a2984|ASV
Parastagonospora nodorum|72b78446d3fe20f7971591ab06dbc924|ASV
Parastagonospora nodorum|KF251177
Parastagonospora nodorum|07c08628c72eab998d7deeef900c3608|ASV
Parastagonospora novozelandica|96c277954dababa319133a8ef9a46459|ASV
Parastagonospora novozelandica|MK539957
Claviceps arundinis|81e93a31d45c370b594cfbaf4fd1c775|ASV
Claviceps arundinis|8d44bd7b74ca85ce6fa16b69832d3a7f|ASV
Claviceps arundinis|MH477791
Zymoseptoria brevis|a5c7c6f934daf6fd81a58d573958b0d0|ASV
Zymoseptoria brevis|JF700867
Blumeria graminis|AB273553
Blumeria graminis|AB273565
Blumeria graminis|1090371c98426dffd36f3d9276453f2d|ASV
Blumeria graminis|AB273563
Blumeria graminis|AJ313140
Blumeria graminis|AB000935
Blumeria graminis|14b45c07661dd1589f112c5bf8e12e72|ASV
Blumeria graminis|AJ313137
Blumeria graminis|4e17e6416d33683730c277337896dce1|ASV
Blumeria graminis|AJ313138
Blumeria graminis|MT462306
Blumeria graminis|MW079022
Blumeria graminis|MW079019
Ustilago maydis|251274bd0490e94be3013cb38132593c|ASV
Ustilago maydis|UDB016255
Ustilago kummeri|KY929592
Ustilago kummeri|8d163e9ea883aeecbc003f99d73a23ff|ASV
Ustilago kummeri|a394505cd26763a85ea5ac9cbe553dcf|ASV
Ustilago coicis|d94896acc5ceceaf8d50883e1890d931|ASV
Ustilago coicis|c7c79c7343cde2318f0d05cfa71ccd57|ASV
Ustilago coicis|5b4f625cd289a49c5f68416713b7129e|ASV
Ustilago coicis|MW320518
Ustilago hordei|4ebd40ed727091280ba68956eea37ac6|ASV
Ustilago hordei|5d621ae28e51de7887c1062647487a5a|ASV
Ustilago hordei|cd84e351e73d5ac62f89c1c61efdb2f7|ASV
Ustilago hordei|AY740068
Ustilago nunavutica|8fa125ed755040eaa4a9133d35a36af5|ASV
Ustilago nunavutica|6086991580adfa6d7842044717af51ed|ASV
Ustilago nunavutica|ed3d45581d8fb1d816af7e0c247134f3|ASV
Ustilago nunavutica|1f9638026f59380c1243307ca60493a3|ASV
Ustilago nunavutica|167aeaf30db2168ebfa53bd740b6d12c|ASV

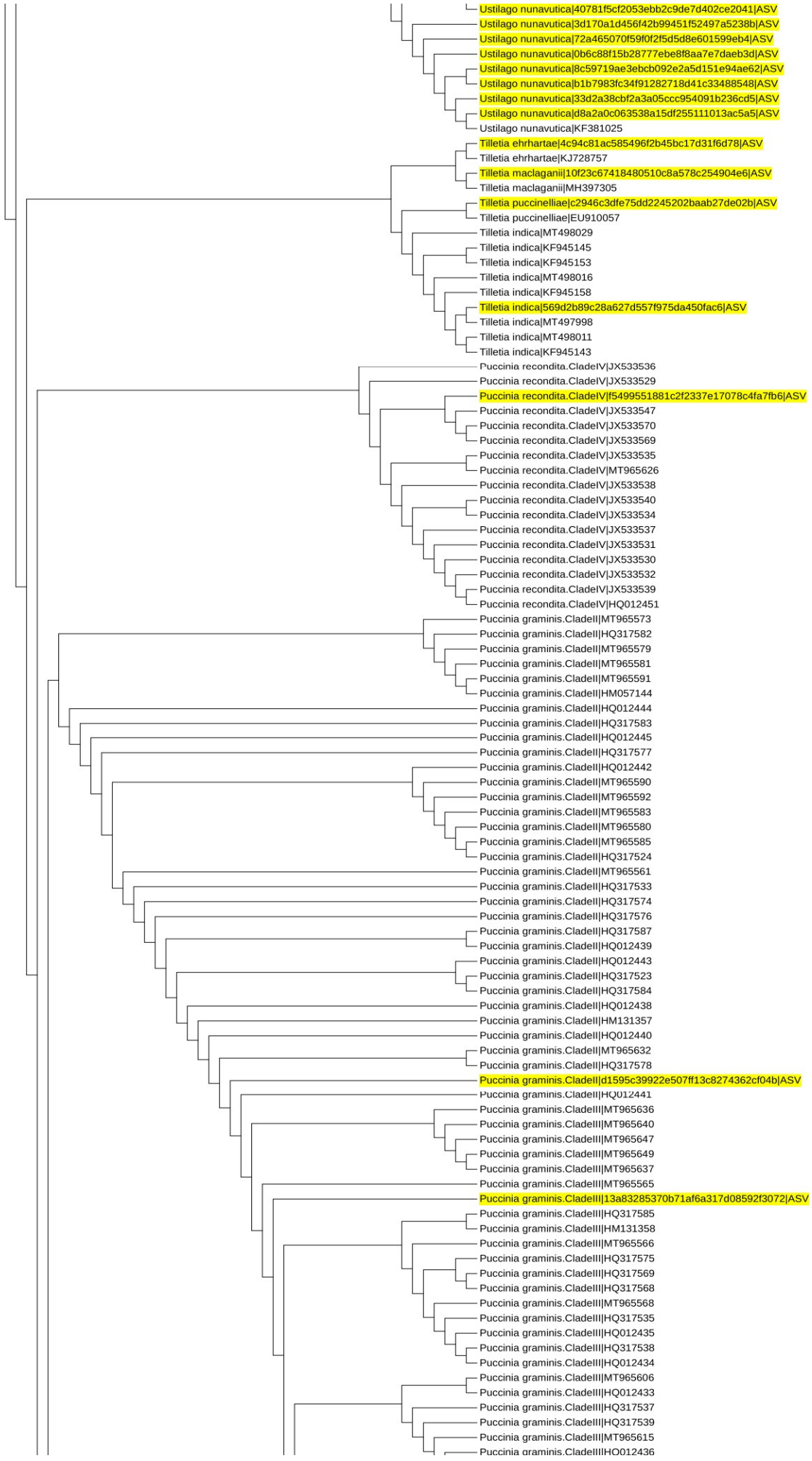
Ustilago nunavutica|40781f5cf2053ebb2c9de7d402ce2041|ASV
Ustilago nunavutica|3d170a1d456f42b99451f52497a5238b|ASV
Ustilago nunavutica|72a465070f59f0f2f5d5d8e601599eb4|ASV
Ustilago nunavutica|0b6c88f15b28777ebe8f8aa7e7daeb3d|ASV
Ustilago nunavutica|8c59719ae3ebcb092e2a5d151e94ae62|ASV
Ustilago nunavutica|b1b7983fc34f91282718d41c33488548|ASV
Ustilago nunavutica|33d2a38cbf2a3a05ccc954091b236cd5|ASV
Ustilago nunavutica|d8a2a0c063538a15df255111013ac5a5|ASV
Ustilago nunavutica|KF381025
Tilletia ehrhartae|4c94c81ac585496f2b45bc17d31f6d78|ASV
Tilletia ehrhartae|KJ728757
Tilletia maclaganii|10f23c67418480510c8a578c254904e6|ASV
Tilletia maclaganii|MH397305
Tilletia puccinelliae|c2946c3dfe75dd2245202baab27de02b|ASV
Tilletia puccinelliae|EU910057
Tilletia indica|MT498029
Tilletia indica|KF945145
Tilletia indica|KF945153
Tilletia indica|MT498016
Tilletia indica|KF945158
Tilletia indica|569d2b89c28a627d557f975da450fac6|ASV
Tilletia indica|MT497998
Tilletia indica|MT498011
Tilletia indica|KF945143
Puccinia recondita.CladeIV|JX533536
Puccinia recondita.CladeIV|JX533529
Puccinia recondita.CladeIV|f5499551881c2f2337e17078c4fa7fb6|ASV
Puccinia recondita.CladeIV|JX533547
Puccinia recondita.CladeIV|JX533570
Puccinia recondita.CladeIV|JX533569
Puccinia recondita.CladeIV|JX533535
Puccinia recondita.CladeIV|MT965626
Puccinia recondita.CladeIV|JX533538
Puccinia recondita.CladeIV|JX533540
Puccinia recondita.CladeIV|JX533534
Puccinia recondita.CladeIV|JX533537
Puccinia recondita.CladeIV|JX533531
Puccinia recondita.CladeIV|JX533530
Puccinia recondita.CladeIV|JX533532
Puccinia recondita.CladeIV|JX533539
Puccinia recondita.CladeIV|HQ012451
Puccinia graminis.CladeII|MT965573
Puccinia graminis.CladeII|HQ317582
Puccinia graminis.CladeII|MT965579
Puccinia graminis.CladeII|MT965581
Puccinia graminis.CladeII|MT965591
Puccinia graminis.CladeII|HM057144
Puccinia graminis.CladeII|HQ012444
Puccinia graminis.CladeII|HQ317583
Puccinia graminis.CladeII|HQ012445
Puccinia graminis.CladeII|HQ317577
Puccinia graminis.CladeII|HQ012442
Puccinia graminis.CladeII|MT965590
Puccinia graminis.CladeII|MT965592
Puccinia graminis.CladeII|MT965583
Puccinia graminis.CladeII|MT965580
Puccinia graminis.CladeII|MT965585
Puccinia graminis.CladeII|HQ317524
Puccinia graminis.CladeII|MT965561
Puccinia graminis.CladeII|HQ317533
Puccinia graminis.CladeII|HQ317574
Puccinia graminis.CladeII|HQ317576
Puccinia graminis.CladeII|HQ317587
Puccinia graminis.CladeII|HQ012439
Puccinia graminis.CladeII|HQ012443
Puccinia graminis.CladeII|HQ317523
Puccinia graminis.CladeII|HQ317584
Puccinia graminis.CladeII|HQ012438
Puccinia graminis.CladeII|HM131357
Puccinia graminis.CladeII|HQ012440
Puccinia graminis.CladeII|MT965632
Puccinia graminis.CladeII|HQ317578
Puccinia graminis.CladeII|d1595c39922e507ff13c8274362cf04b|ASV
Puccinia graminis.CladeII|HQ012441
Puccinia graminis.CladeIII|MT965636
Puccinia graminis.CladeIII|MT965640
Puccinia graminis.CladeIII|MT965647
Puccinia graminis.CladeIII|MT965649
Puccinia graminis.CladeIII|MT965637
Puccinia graminis.CladeIII|MT965565
Puccinia graminis.CladeIII|13a83285370b71af6a317d08592f3072|ASV
Puccinia graminis.CladeIII|HQ317585
Puccinia graminis.CladeIII|HM131358
Puccinia graminis.CladeIII|MT965566
Puccinia graminis.CladeIII|HQ317575
Puccinia graminis.CladeIII|HQ317569
Puccinia graminis.CladeIII|HQ317568
Puccinia graminis.CladeIII|MT965568
Puccinia graminis.CladeIII|HQ317535
Puccinia graminis.CladeIII|HQ012435
Puccinia graminis.CladeIII|HQ317538
Puccinia graminis.CladeIII|HQ012434
Puccinia graminis.CladeIII|MT965606
Puccinia graminis.CladeIII|HQ012433
Puccinia graminis.CladeIII|HQ317537
Puccinia graminis.CladeIII|HQ317539
Puccinia graminis.CladeIII|MT965615
Puccinia graminis.CladeIII|HQ012436

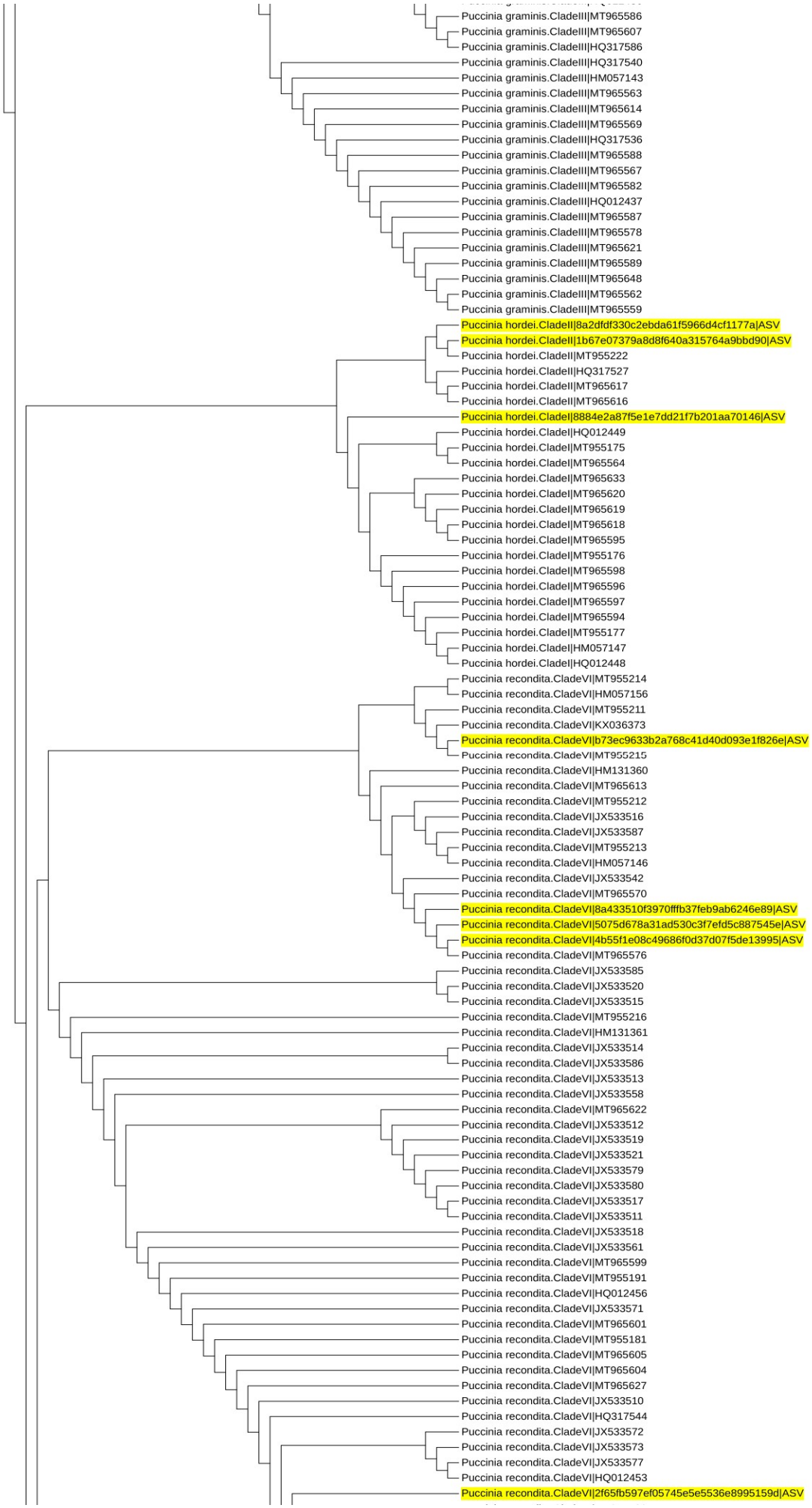
Puccinia graminis.CladeIII|MT965586
Puccinia graminis.CladeIII|MT965607
Puccinia graminis.CladeIII|HQ317586
Puccinia graminis.CladeIII|HQ317540
Puccinia graminis.CladeIII|HM057143
Puccinia graminis.CladeIII|MT965563
Puccinia graminis.CladeIII|MT965614
Puccinia graminis.CladeIII|MT965569
Puccinia graminis.CladeIII|HQ317536
Puccinia graminis.CladeIII|MT965588
Puccinia graminis.CladeIII|MT965567
Puccinia graminis.CladeIII|MT965582
Puccinia graminis.CladeIII|HQ012437
Puccinia graminis.CladeIII|MT965587
Puccinia graminis.CladeIII|MT965578
Puccinia graminis.CladeIII|MT965621
Puccinia graminis.CladeIII|MT965589
Puccinia graminis.CladeIII|MT965648
Puccinia graminis.CladeIII|MT965562
Puccinia graminis.CladeIII|MT965559
Puccinia hordei.CladeII|8a2dfdf330c2ebda61f5966d4cf1177a|ASV
Puccinia hordei.CladeII|1b67e07379a8d8f640a315764a9bbd90|ASV
Puccinia hordei.CladeII|MT955222
Puccinia hordei.CladeII|HQ317527
Puccinia hordei.CladeII|MT965617
Puccinia hordei.CladeII|MT965616
Puccinia hordei.CladeI|8884e2a87f5e1e7dd21f7b201aa70146|ASV
Puccinia hordei.CladeI|HQ012449
Puccinia hordei.CladeI|MT955175
Puccinia hordei.CladeI|MT965564
Puccinia hordei.CladeI|MT965633
Puccinia hordei.CladeI|MT965620
Puccinia hordei.CladeI|MT965619
Puccinia hordei.CladeI|MT965618
Puccinia hordei.CladeI|MT965595
Puccinia hordei.CladeI|MT955176
Puccinia hordei.CladeI|MT965598
Puccinia hordei.CladeI|MT965596
Puccinia hordei.CladeI|MT965597
Puccinia hordei.CladeI|MT965594
Puccinia hordei.CladeI|MT955177
Puccinia hordei.CladeI|HM057147
Puccinia hordei.CladeI|HQ012448
Puccinia recondita.CladeVI|MT955214
Puccinia recondita.CladeVI|HM057156
Puccinia recondita.CladeVI|MT955211
Puccinia recondita.CladeVI|KX036373
Puccinia recondita.CladeVI|b73ec9633b2a768c41d40d093e1f826e|ASV
Puccinia recondita.CladeVI|MT955215
Puccinia recondita.CladeVI|HM131360
Puccinia recondita.CladeVI|MT965613
Puccinia recondita.CladeVI|MT955212
Puccinia recondita.CladeVI|JX533516
Puccinia recondita.CladeVI|JX533587
Puccinia recondita.CladeVI|MT955213
Puccinia recondita.CladeVI|HM057146
Puccinia recondita.CladeVI|JX533542
Puccinia recondita.CladeVI|MT965570
Puccinia recondita.CladeVI|8a433510f3970fffb37feb9ab6246e89|ASV
Puccinia recondita.CladeVI|5075d678a31ad530c3f7efd5c887545e|ASV
Puccinia recondita.CladeVI|4b55f1e08c49686f0d37d07f5de13995|ASV
Puccinia recondita.CladeVI|MT965576
Puccinia recondita.CladeVI|JX533585
Puccinia recondita.CladeVI|JX533520
Puccinia recondita.CladeVI|JX533515
Puccinia recondita.CladeVI|MT955216
Puccinia recondita.CladeVI|HM131361
Puccinia recondita.CladeVI|JX533514
Puccinia recondita.CladeVI|JX533586
Puccinia recondita.CladeVI|JX533513
Puccinia recondita.CladeVI|JX533558
Puccinia recondita.CladeVI|MT965622
Puccinia recondita.CladeVI|JX533512
Puccinia recondita.CladeVI|JX533519
Puccinia recondita.CladeVI|JX533521
Puccinia recondita.CladeVI|JX533579
Puccinia recondita.CladeVI|JX533580
Puccinia recondita.CladeVI|JX533517
Puccinia recondita.CladeVI|JX533511
Puccinia recondita.CladeVI|JX533518
Puccinia recondita.CladeVI|JX533561
Puccinia recondita.CladeVI|MT965599
Puccinia recondita.CladeVI|MT955191
Puccinia recondita.CladeVI|HQ012456
Puccinia recondita.CladeVI|JX533571
Puccinia recondita.CladeVI|MT965601
Puccinia recondita.CladeVI|MT955181
Puccinia recondita.CladeVI|MT965605
Puccinia recondita.CladeVI|MT965604
Puccinia recondita.CladeVI|MT965627
Puccinia recondita.CladeVI|JX533510
Puccinia recondita.CladeVI|HQ317544
Puccinia recondita.CladeVI|JX533572
Puccinia recondita.CladeVI|JX533573
Puccinia recondita.CladeVI|JX533577
Puccinia recondita.CladeVI|HQ012453
Puccinia recondita.CladeVI|2f65fb597ef05745e5e5536e8995159d|ASV

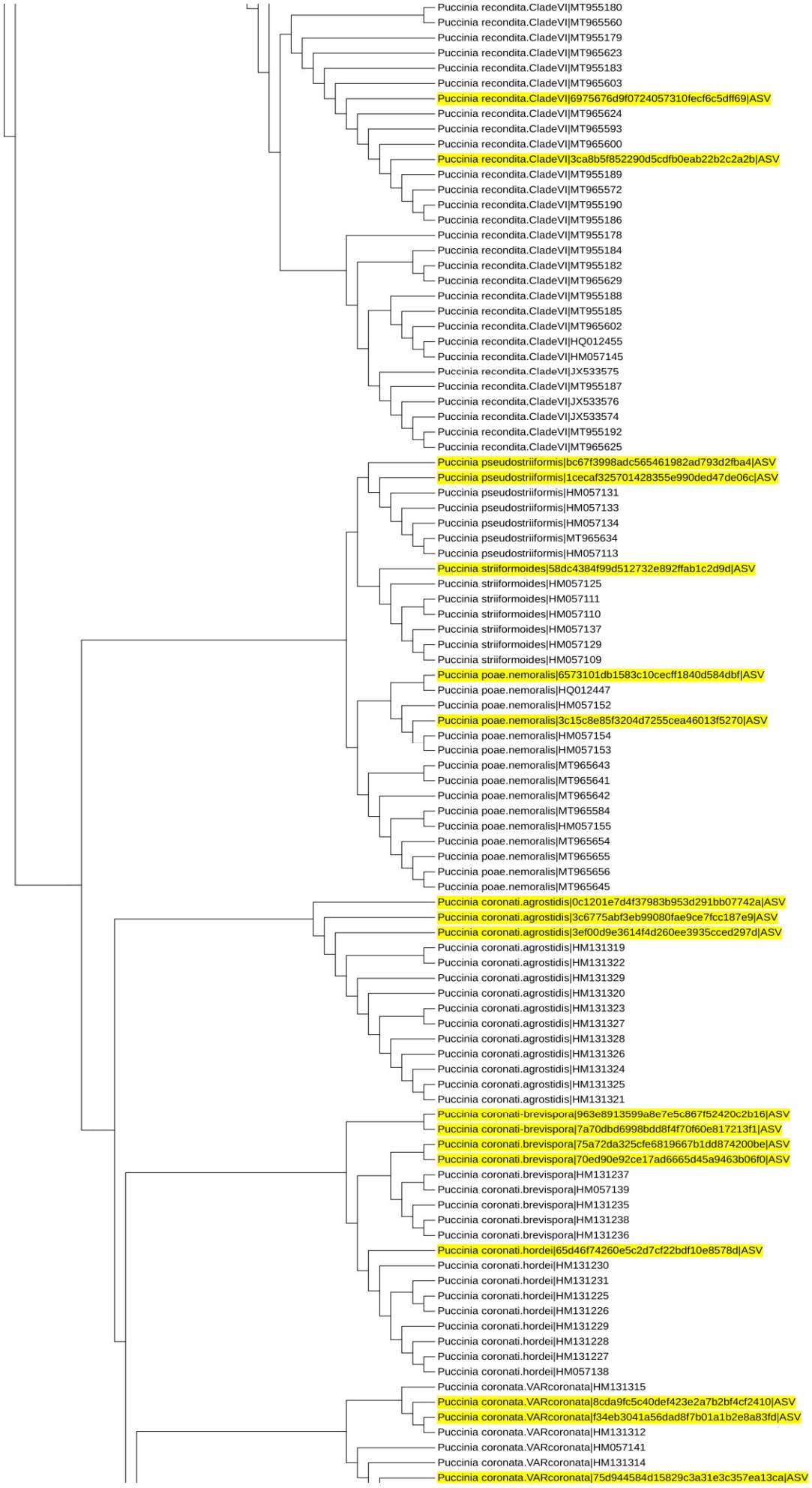
Puccinia recondita.CladeVI|MT955180
Puccinia recondita.CladeVI|MT965560
Puccinia recondita.CladeVI|MT955179
Puccinia recondita.CladeVI|MT965623
Puccinia recondita.CladeVI|MT955183
Puccinia recondita.CladeVI|MT965603
Puccinia recondita.CladeVI|6975676d9f0724057310fecf6c5dff69|ASV
Puccinia recondita.CladeVI|MT965624
Puccinia recondita.CladeVI|MT965593
Puccinia recondita.CladeVI|MT965600
Puccinia recondita.CladeVI|3ca8b5f852290d5cdfb0eab22b2c2a2b|ASV
Puccinia recondita.CladeVI|MT955189
Puccinia recondita.CladeVI|MT965572
Puccinia recondita.CladeVI|MT955190
Puccinia recondita.CladeVI|MT955186
Puccinia recondita.CladeVI|MT955178
Puccinia recondita.CladeVI|MT955184
Puccinia recondita.CladeVI|MT955182
Puccinia recondita.CladeVI|MT965629
Puccinia recondita.CladeVI|MT955188
Puccinia recondita.CladeVI|MT955185
Puccinia recondita.CladeVI|MT965602
Puccinia recondita.CladeVI|HQ012455
Puccinia recondita.CladeVI|HM057145
Puccinia recondita.CladeVI|JX533575
Puccinia recondita.CladeVI|MT955187
Puccinia recondita.CladeVI|JX533576
Puccinia recondita.CladeVI|JX533574
Puccinia recondita.CladeVI|MT955192
Puccinia recondita.CladeVI|MT965625
Puccinia pseudostriiformis|bc67f3998adc565461982ad793d2fba4|ASV
Puccinia pseudostriiformis|1cecaf325701428355e990ded47de06c|ASV
Puccinia pseudostriiformis|HM057131
Puccinia pseudostriiformis|HM057133
Puccinia pseudostriiformis|HM057134
Puccinia pseudostriiformis|MT965634
Puccinia pseudostriiformis|HM057113
Puccinia striiformoides|58dc4384f99d512732e892ffab1c2d9d|ASV
Puccinia striiformoides|HM057125
Puccinia striiformoides|HM057111
Puccinia striiformoides|HM057110
Puccinia striiformoides|HM057137
Puccinia striiformoides|HM057129
Puccinia striiformoides|HM057109
Puccinia poae.nemoralis|6573101db1583c10cecff1840d584dbf|ASV
Puccinia poae.nemoralis|HQ012447
Puccinia poae.nemoralis|HM057152
Puccinia poae.nemoralis|3c15c8e85f3204d7255cea46013f5270|ASV
Puccinia poae.nemoralis|HM057154
Puccinia poae.nemoralis|HM057153
Puccinia poae.nemoralis|MT965643
Puccinia poae.nemoralis|MT965641
Puccinia poae.nemoralis|MT965642
Puccinia poae.nemoralis|MT965584
Puccinia poae.nemoralis|HM057155
Puccinia poae.nemoralis|MT965654
Puccinia poae.nemoralis|MT965655
Puccinia poae.nemoralis|MT965656
Puccinia poae.nemoralis|MT965645
Puccinia coronati.agrostidis|0c1201e7d4f37983b953d291bb07742a|ASV
Puccinia coronati.agrostidis|3c6775abf3eb99080fae9ce7fcc187e9|ASV
Puccinia coronati.agrostidis|3ef00d9e3614f4d260ee3935cced297d|ASV
Puccinia coronati.agrostidis|HM131319
Puccinia coronati.agrostidis|HM131322
Puccinia coronati.agrostidis|HM131329
Puccinia coronati.agrostidis|HM131320
Puccinia coronati.agrostidis|HM131323
Puccinia coronati.agrostidis|HM131327
Puccinia coronati.agrostidis|HM131328
Puccinia coronati.agrostidis|HM131326
Puccinia coronati.agrostidis|HM131324
Puccinia coronati.agrostidis|HM131325
Puccinia coronati.agrostidis|HM131321
Puccinia coronati-brevispora|963e8913599a8e7e5c867f52420c2b16|ASV
Puccinia coronati-brevispora|7a70dbd6998bdd8f4f70f60e817213f1|ASV
Puccinia coronati.brevispora|75a72da325cfe6819667b1dd874200be|ASV
Puccinia coronati.brevispora|70ed90e92ce17ad6665d45a9463b06f0|ASV
Puccinia coronati.brevispora|HM131237
Puccinia coronati.brevispora|HM057139
Puccinia coronati.brevispora|HM131235
Puccinia coronati.brevispora|HM131238
Puccinia coronati.brevispora|HM131236
Puccinia coronati.hordei|65d46f74260e5c2d7cf22bdf10e8578d|ASV
Puccinia coronati.hordei|HM131230
Puccinia coronati.hordei|HM131231
Puccinia coronati.hordei|HM131225
Puccinia coronati.hordei|HM131226
Puccinia coronati.hordei|HM131229
Puccinia coronati.hordei|HM131228
Puccinia coronati.hordei|HM131227
Puccinia coronati.hordei|HM057138
Puccinia coronata.VARcoronata|HM131315
Puccinia coronata.VARcoronata|8cda9fc5c40def423e2a7b2bf4cf2410|ASV
Puccinia coronata.VARcoronata|f34eb3041a56dad8f7b01a1b2e8a83fd|ASV
Puccinia coronata.VARcoronata|HM131312
Puccinia coronata.VARcoronata|HM057141
Puccinia coronata.VARcoronata|HM131314
Puccinia coronata.VARcoronata|75d944584d15829c3a31e3c357ea13ca|ASV

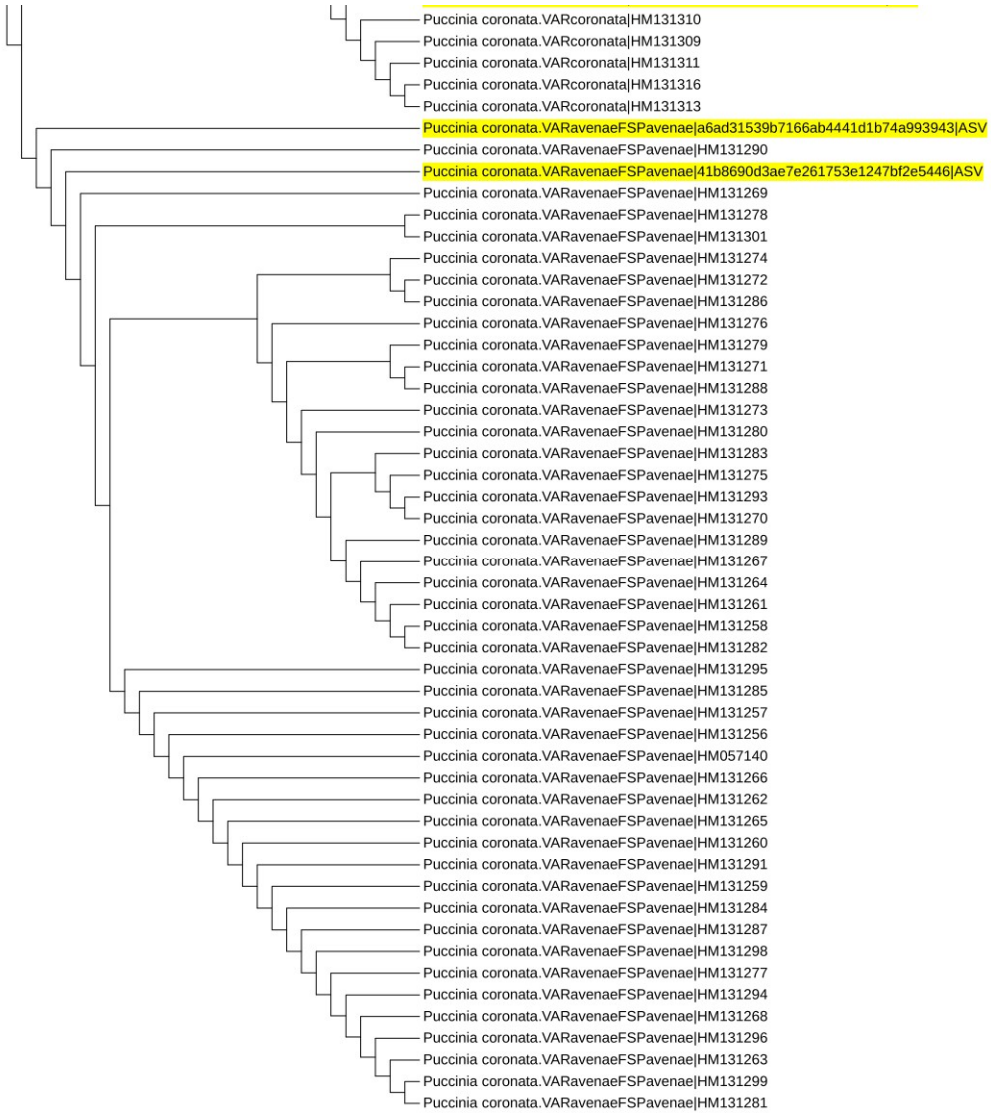

Figure S10. Reconstructed tree used for species-level classifications. Names highlighted in yellow are the ASVs from the sample data.